Atmospheric
Chemistry
and Physics

Characterization of biogenic volatile organic compounds and their oxidation products in a stressed spruce-dominated forest close to a biogas power plant

Junwei Song[1,4], **Georgios I. Gkatzelis**[2], **Ralf Tillmann**[2], **Nicolas Brüggemann**[3], **Thomas Leisner**[1], **and Harald Saathoff**[1]

[1]Institute of Meteorology and Climate Research, Karlsruhe Institute of Technology,
Hermann-von-Helmholtz-Platz 1, 76344 Eggenstein-Leopoldshafen, Germany
[2]Institute of Energy and Climate Research, IEK-8: Troposphere,
Forschungszentrum Jülich GmbH, 52425 Jülich, Germany
[3]Institute of Bio- and Geosciences, IBG-3: Agrosphere, Forschungszentrum
Jülich GmbH, 52425 Jülich, Germany
[4]Université Claude Bernard Lyon 1, CNRS, IRCELYON, UMR 5256, 69626 Villeurbanne, France

Correspondence: Junwei Song (junwei.song@ircelyon.univ-lyon1.fr) and Harald Saathoff
(harald.saathoff@kit.edu)

Abstract. Biogenic volatile organic compounds (BVOCs) are key components of the atmosphere, playing a significant role in the formation of organic aerosols (OAs). However, only a few studies have simultaneously examined the characteristics of BVOCs and OAs in forest ecosystems on the background of environmental stressors, such as consecutive droughts and extensive bark beetle infestations. Here, we present real-time measurements of OAs and BVOCs in a stressed spruce-dominated forest near a biogas power plant (BPP) in western Germany during June 2020. A proton-transfer-reaction time-of-flight mass spectrometer coupled with a particle inlet (CHARON-PTR-ToF-MS) and a Vocus-PTR-ToF-MS were used to measure OAs and BVOCs. The average OA mass concentration was $0.8 \pm 0.5\,\mu g\,m^{-3}$, consisting mainly of semi-volatile monoterpene oxidation products. The average mixing ratios of isoprene (0.58 ± 0.54 ppb) and monoterpenes (2.5 ± 5.3 ppb) were higher than the values previously measured in both German temperate forests and boreal forests. Based on a wind direction analysis, BVOC data were categorized into two groups: one mainly influenced by biogenic emissions from an intact forest and a clear-cut area (referred to as the biogenic group) and the other mainly influenced by anthropogenic emissions from a BPP and a village (referred to as the anthropogenic group). High mixing ratios of monoterpenes were observed in the anthropogenic group, indicating a significant contribution of BPP emissions. In the biogenic group, the variations in BVOC mixing ratios were driven by the interplay between meteorology, biogenic emissions and their photochemical consumption. Positive matrix factorization analysis of VOCs revealed substantial contributions of oxygenated organic compounds from the photochemical oxidation of BVOCs during daytime, while monoterpenes and their weakly oxidized products dominated at night. Furthermore, increasing relative humidity and decreasing temperatures promoted the gas-to-particle partitioning of these weakly oxidized monoterpene products, leading to an increase in nighttime OA mass. The results demonstrate that variations in BVOCs are influenced not only by meteorological conditions and biogenic emissions but also by local BPP emissions and subsequent chemical transformation processes. This study highlights the need to investigate the changes in biogenic emissions in stressed European forests.

1 Introduction

Volatile organic compounds (VOCs) play important roles in determining atmospheric chemical processes (Atkinson, 2000; Hallquist et al., 2009; Yáñez-Serrano et al., 2020; Shrivastava et al., 2017; Rasmussen and Went, 1965; Trainer et al., 1987; Peñuelas and Staudt, 2010). Terrestrial ecosystems emit large amounts of biogenic VOCs (BVOCs, $> 1000\,\mathrm{Tg\,yr^{-1}}$) to the global atmosphere, especially compared with anthropogenic VOC (AVOC) emissions ($\sim 200\,\mathrm{Tg\,yr^{-1}}$) (Guenther et al., 2012; Sindelarova et al., 2014). BVOCs emitted by vegetation consist largely of reactive terpenoids, such as isoprene ($\sim 70\,\%$), monoterpenes ($\sim 11\,\%$) and sesquiterpenes ($\sim 2.5\,\%$) (Sindelarova et al., 2014). The oxidation products of terpenoids can nucleate to form new particles or contribute to the growth of existing particles and secondary organic aerosol (SOA) formation, thereby impacting air quality and climate (Hallquist et al., 2009; Shrivastava et al., 2017).

Over the last decade, many field studies have been conducted in different forest ecosystems to investigate the characteristics of BVOCs, including the emissions and temporal variations as well as their impacts on atmospheric reactivity and SOA formation (Hakola et al., 2012; Hellén et al., 2018; Li et al., 2020; Huang et al., 2021; Yáñez-Serrano et al., 2021; Vestenius et al., 2021; Mermet et al., 2021; Vermeuel et al., 2023; Weber et al., 2022; Bourtsoukidis et al., 2024, 2014). The diurnal pattern in isoprene concentrations in forests typically shows higher values during daytime (Yáñez-Serrano et al., 2021; Li et al., 2020; Hakola et al., 2012), as isoprene emissions increase with temperature and sunlight intensity as result of increased de novo production and direct release. In contrast, monoterpenes are mainly released from storage pools of boreal pines. The emission and composition of BVOCs from trees varies with abiotic and biotic stresses, such as high temperature (Teskey et al., 2015; Kleist et al., 2012), drought (Peron et al., 2021; Bonn et al., 2019) and herbivore attack (Jaakkola et al., 2023; Kari et al., 2019; Faiola and Taipale, 2020). It has been reported that these stresses can alter the emissions of BVOCs, especially those of terpenoids (Ghimire et al., 2016; Jaakkola et al., 2023; Byron et al., 2022).

In addition to biogenic emissions, the temporal variations in BVOC concentrations, especially of terpenoids, are influenced by atmospheric oxidation processes. The diurnal variation in monoterpene concentrations shows lower values during daytime than at nighttime in the boreal forests; this has been attributed to rapid photochemical consumption and expanded boundary layer heights (Hellén et al., 2018; Hakola et al., 2012). Correspondingly, higher concentrations of monoterpene oxidation products are expected to be produced during daytime. For instance, Huang et al. (2021) found that some gaseous monoterpene oxidation products, e.g., $C_7H_{10}O_4$ (3,6-oxoheptanoic acid) and $C_8H_{12}O_4$ (terpenylic acid), showed higher concentrations during daytime

in a boreal forest. Li et at. (2020) reported similar diurnal variations in more highly oxidized gaseous monoterpene products (e.g., $C_8H_{12}O_{4-6}$, $C_9H_{14}O_{4-6}$, $C_{10}H_{14}O_{4-6}$ and $C_{10}H_{16}O_{4-6}$) in the French Landes Forest, which is largely composed of maritime pines. The variations in BVOC oxidation products are also influenced by gas–particle partitioning processes. Laboratory studies have shown that decreasing temperature and increasing relative humidity (RH) can lead to an increased particulate fraction of SOA products from BVOC oxidation (Surdu et al., 2023; von Hessberg et al., 2009; Tillmann et al., 2010; Zhang et al., 2015; Luo et al., 2024). However, due to a lack of online dual-phase measurements, only a few field studies have focused on the gas–particle partitioning of BVOC oxidation products in healthy forests (Mohr et al., 2017; Yatavelli et al., 2014; Isaacman-VanWertz et al., 2016; Lee et al., 2018). However, our understanding of the interplay between the gas and particle phases of BVOC oxidation products in a real forest atmosphere, particularly in a stressed forest, remains limited. Addressing these gaps is crucial for assessing the impact of various environmental factors on BVOC emissions and their subsequent transformation (Faiola and Taipale, 2020).

The Eifel is a low mountain range in western Germany that stretches across the federal states of North Rhine-Westphalia and Rhineland-Palatinate and covers an area of $\sim 5300\,\mathrm{km^2}$. The forested areas in this region are largely composed of Norway spruce (*Picea abies* (L.) Karst.), which is an important species with respect to BVOC contributions (Smiatek and Steinbrecher, 2006; Kleist et al., 2012). The Eifel Forest suffered from severe droughts, heat waves and bark beetle infestation in the years before our measurements; thus, here, it serves as a case study to examine BVOC variations in a stressed European coniferous forest. In this study, a field measurement campaign was conducted at a site of the northern Eifel Forest in the vicinity of a biogas power plant (BPP). Europe is the world leader in biogas electricity production, with more than 18 000 BPPs (Brémond et al., 2021). These BPPs are widely distributed in European rural areas close to forests (Bakkaloglu et al., 2021; Scheftelowitz et al., 2018), which periodically emit large amounts of CH_4 and VOCs into the atmosphere around the BPPs (Salazar Gómez et al., 2016). In this paper, we present the real-time measurements of VOCs and aerosol particles measured by a proton-transfer-reaction time-of-flight mass spectrometer (PTR-ToF-MS) coupled with a particle inlet (CHARON, Chemical Analysis of Aerosol Online) and a Vocus-PTR-ToF-MS. The impacts of meteorological conditions, sources and chemical oxidation processes on the variations in BVOCs and their gaseous and particulate oxidation products were investigated to get a better understanding of BVOC emissions and their contributions to SOAs as well as the potential impact of BPP emissions.
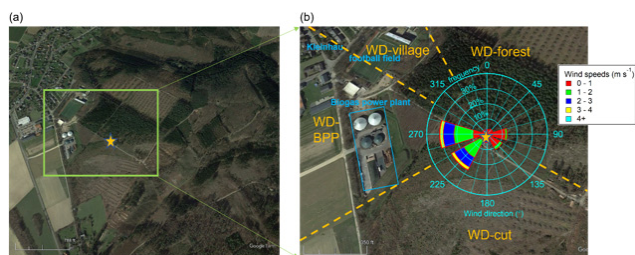
Figure 1. The **(a)** location of the sampling site (orange star) (©Google Earth) and **(b)** a close-up of the sampling site with a centered wind rose for the entire measurement period. The orange dashed lines are shown to distinguish different wind direction (WD) sectors: the WD-forest at 0–120° is influenced by an intact forest area, the WD-cut at 120–240° is influenced by a clear-cut area, the WD-BPP at 240–300° is influenced by a biogas power plant (blue rectangle) and the WD-village at 300–330° is influenced by residential areas of Kleinhau.

2 Methods

2.1 Sampling site

In this study, a 3-week field campaign was conducted at a site in the northern Eifel Forest (50.72° N, 6.40° E) during June 2020 as a part of the "Heat and Drought 2020" campaign of the Modular Observation Solutions of Earth Systems (MOSES) project run by the Helmholtz Association of German Research Centers. The Eifel Forest had been suffering from severe droughts, heat waves and severe bark beetle infestation in the lead-up to the study (Weber et al., 2022; Ghimire et al., 2016). Within a 2-year period (2018–2020), 14 % of the spruce trees in the northern Eifel region were removed due to summer droughts, and only 28.3 % remained in good condition (Montzka et al., 2021). Therefore, the Eifel Forest can serve as an example of a stressed temperate coniferous forest.

As shown in Fig. 1, the measurement site was situated directly next to a stand of Norway spruce, with a few shrubs and blueberry plants also surrounding the area. To the south and southeast of the measurements site, there were some clear-cut areas due to bark beetle infestation in the period from 2018 to 2020. Additionally, the measurement site was located ~ 400 m southeast of a football field in the small village Kleinhau, Germany, belonging to the municipality of Hürtgenwald (population of about 9000) and ~ 250 m east of a BPP (Bioenergie Kleinhau GmbH, Hürtgen, Germany). The biomass substrate used for the biogas production in this BPP consisted mainly of crop waste (e.g., corn stover). The measurement site was affected by the BPP emissions, especially under westerly wind conditions.

2.2 Instrumentation

All instruments were set up in a temperature-controlled measurement container (~ 25 °C) located at the sampling site. All sampling inlets were located 3.7 m above ground level and 1 m above the container roof. An overview of instruments and parameters measured is given in Table S1 in the Supplement.

A PTR-ToF-MS 4000X2 coupled with a CHARON particle inlet (IONICON Analytik GmbH, Innsbruck, Austria) was deployed to measure VOCs and aerosol particles from 5 to 30 June 2020. A detailed description of the PTR-ToF-MS and CHARON inlet has been provided elsewhere (Jordan et al., 2009; Müller et al., 2017; Eichler et al., 2015). Briefly, CHARON consists of a charcoal denuder for stripping off gaseous organics, an aerodynamic lens for enriching particles, and a thermodesorption unit for particle evaporation prior to chemical analysis by PTR-ToF-MS. In this campaign, both gases and particles were measured by switching between different modes with the IoniTOF 4.0 data acquisition software (IONICON Analytik GmbH, Innsbruck, Austria). Specifically, one alternating measurement cycle included 3 min in high-efficiency particulate-air (HEPA) filter mode to measure the particle background, 1 min in transition mode to establish instrument equilibrium, 10 min in CHARON mode to measure particle-phase compounds, another 1 min in transition mode and 10 min in VOC mode to measure gas-phase compounds (Fig. S1 in the Supplement). A 1 min transition time is sufficient for the equilibrium of instrumental conditions between different modes (Piel et al., 2021). During the gas-phase measurement, ambient air was sampled continuously from a 3 m long perfluoroalkoxy tube (1/4 in. inner diameter) with a total flow rate of 1.45 L min^{-1}, and a subset flow of ~ 0.1 L min^{-1} was then sampled by the PTR-MS through a polyetheretherketone tube maintained at 80 °C. During the particle-phase measurement, ambient particles were sampled by a PM$_{2.5}$ inlet with a flow rate of 16.7 L min^{-1}, out of which a flow of 0.55 L min^{-1} was directed to the CHARON inlet maintained by a vacuum pump (ACP15, Pfeiffer Vacuum, Germany). During a first measurement stage from 5 to 19 June, the PTR drift tube was set with alternating temperatures at 80 and 120 °C for the gas- and particle-phase measurement modes, respectively. With these settings, the actual drift tube temperatures varied during the gas and particle measurement modes, thereby complicating the data analysis (Figs. S1 and S2). During a second measurement stage from 22 to 30 June, the PTR drift tube was set with the same temperature of 120 °C and a drift tube pressure of 2.7 mbar for both gas and particle measurement modes. The CHARON inlet was set to a thermodesorption unit temperature of 150 °C and a pressure of 7–8 mbar. Finally, the electric field (E/N where E is the electric field strength and N is the buffer gas density) of the CHARON-PTR-ToF-MS was kept at ~ 97 and ~ 57 Td for the gas- and particle-phase measurement modes, respectively, during the second measurement stage. Please note that the actual temperature of the drift tube fluctuated during the first measurement stage and was lower than the intended temperature of 120 °C (Fig. S1). This made it dif-

ficult to quantify organic compounds in the particle phase measured by the CHARON-PTR-ToF-MS. For the gas-phase measurements, we corrected the major VOC data from the first measurement stage based on gas calibration and cross-comparison with Vocus-PTR-ToF-MS measurements. Consequently, we can present the major VOC species measured by the CHARON-PTR-ToF-MS for the entire campaign, but the particle-phase data for first measurement stage have been excluded from further analysis in this study.

Gas calibrations of CHARON-PTR-ToF-MS were performed via dynamic dilution of a calibration gas cylinder containing 11 VOC species (Table S2; accuracy of 10 % at ~ 100 ppb). The VOC background was taken from zero-air measurements during the gas calibrations at the beginning and the end of the campaign. The enrichment factor of the CHARON inlet was determined using an external calibration with size-selected ammonium nitrate particles (NH_4NO_3) that were counted using a condensation particle counter (CPC3772, TSI Inc., Shoreview, MN, USA). The enrichment factor was determined with an average value of 18 ± 2 in the 150–700 nm particle size range, with lower values for smaller particles below 150 nm (Fig. S3). The particle background was determined using a HEPA filter (ETA filter model HC01-5N-B, Aerocolloid LLC, Minneapolis, MN, USA) that was placed upstream of the gas-phase denuder of the CHARON inlet. All data files recorded by the CHARON-PTR-ToF-MS were processed using the IONICON software Data Analyzer (IDA version1.0.0.2, IONICON Analytik GmbH, Innsbruck, Austria). More details regarding the data processing with the IDA are given in Sect. S1 in the Supplement.

A Vocus-PTR-ToF-MS (Aerodyne Research Inc., Billerica, MA, USA) was deployed to measure VOCs and oxygenated VOCs concurrently with the CHARON-PTR-ToF-MS from 10 to 30 June. The Vocus-PTR-ToF-MS was not available for measurements before 10 June 2020 due to a technical problem. The details of the Vocus-PTR-ToF-MS have been described elsewhere (Krechmer et al., 2018). The Vocus-PTR-ToF-MS is characterized by a newly designed reagent-ion source and a focusing ion–molecule reactor (FIMR), both of which improve the detection efficiency of ions. In this study, the FIMR was operated at a pressure of 1.5 mbar. The mass-resolving power of the ToF mass analyzer was $\sim 10\,000$ amu/Δamu (where amu denotes atomic mass units). Raw data were recorded with a time resolution of 5 s. For the Vocus-PTR-ToF-MS measurement, ambient air was drawn in through a 1 m long PFA tubing with a total flow rate of 4.5 L min^{-1}, and a subset flow of 0.1–0.15 L min^{-1} then went into the Vocus-PTR-ToF-MS. Background measurements using high-purity nitrogen were automatically performed every hour. The Vocus-PTR-ToF-MS was regularly calibrated using a homemade gas standard of 15 compounds at ~ 1 ppmv with an accuracy of 10 % (Table S2). At the end of the campaign, a gas cross-calibration was performed between the Vocus-PTR-ToF-MS and CHARON-PTR-ToF-MS with the calibration gas cylin-

der (IONICON Analytik GmbH). The Vocus-PTR-ToF-MS data analysis was performed using the Tofware software package (AG, Thun, Switzerland). For the quantification of uncalibrated species measured by the Vocus-PTR-ToF-MS, we adopted the rate constants of proton transfer reactions (K_{cap}) from the PTR library (Pagonis et al., 2019). We then generated a sensitivity for the uncalibrated masses by applying a correction factor based on the k_{cap} ratios to the calibrated masses. Finally, the Vocus-PTR-ToF-MS data were synchronized to the measurement time of the CHARON-PTR-ToF-MS for comparison of the VOC data. In this study, a series of VOC species were simultaneously detected by the CHARON-PTR-ToF-MS and the Vocus-PTR-ToF-MS; a detailed comparison is provided in Sect. S2.

In addition, methane (CH_4), carbon dioxide (CO_2), water vapor (H_2O) and carbon monoxide (CO) were measured with a cavity ring-down spectrometer (G2401; Picarro, Santa Clara, CA, USA) from 10 to 30 June. O_3 was measured using a commercial chemiluminescence analyzer (Cranox II, ECO PHYSICS GmbH, Hürth, Germany). An optical particle counter (OPC, Fidas200, Palas GmbH, Karlsruhe, Germany) was used to measure the mass concentrations of $PM_{2.5}$ and PM_{10} from 5 to 30 June. Simultaneously, black carbon (BC) concentrations were measured with an Aethalometer (MA200, AethLabs, CA, USA). Particle number concentrations were measured with a condensation particle counter (CPC3776, TSI Inc., Shoreview, MN, USA). A nanoparticle sizer (NanoScan SMPS, TSI3910, TSI Inc., Shoreview, MN, USA) was used to measure the particle number size distribution between 10 and 410 nm.

Meteorological parameters were measured by a compact sensor (WS700, Lufft GmbH, Fellbach, Germany). The meteorological data were missing during some short periods due to data acquisition malfunctions. We also used hourly data of temperature, relative humidity, precipitation and planetary boundary layer (PBL) height from the European Centre for Medium-Range Weather Forecasts' ERA5 reanalysis (Hersbach et al., 2020) as well as wind speed and direction data from the NASA POWER Data Access Viewer (https://power.larc.nasa.gov/, last access: 10 October 2023) to complement the meteorological data. The daily soil moisture was measured by a cosmic-ray neutron sensor (CRNS) (Bogena et al., 2015), which was located ~ 150 m southwest of the sampling site. In addition, the spatial distribution of soil moisture in the northern Eifel Forest was determined from CRNS rover measurements.

2.3 Positive matrix factorization (PMF) analysis

The PMF receptor model is a bilinear analytic algorithm that separates the time series of air pollutants into different sources represented by factor profiles, factor time series and residual signals (Paatero and Tapper, 1994). The PMF model has been widely used to determine different sources and chemical processes of VOCs measured by the PTR-ToF-MS

in urban, rural and forest atmospheres (Gkatzelis et al., 2021; H. Li et al., 2021; Wang et al., 2020; Li et al., 2022; Pernov et al., 2021; Desservettaz et al., 2023; Jain et al., 2023; Song et al., 2024a). To explore the sources and chemical processes of VOCs, we performed a PMF analysis of VOC species measured by the Vocus-PTR-ToF-MS, rather than those measured by CHARON-PTR-ToF-MS. This is mainly due to the fact that the Vocus-PTR-ToF-MS can measure higher-molecular-weight OVOCs ($m/z > 200$) well, thereby providing more information for interpreting the oxidation processes of BVOCs (H. Li et al., 2021).

In this study, the Vocus-PTR-ToF-MS-measured VOC ions with a chemical formula assignment (mainly $C_xH_y^+$ and $C_xH_yO_z^+$) were selected to perform the PMF analysis. The PMF input data were prepared according to the protocol reported in previous studies (Pernov et al., 2021; Li et al., 2022). The uncertainties were calculated with the following equations:

$$\text{Unc.} = \begin{cases} \text{LOD} \times \frac{5}{6} & \text{conc.} \leq \text{LOD}, \quad (1) \\ \sqrt{\text{LOD}^2 + (\text{error fraction} \times \text{conc.})^2} & \text{conc.} > \text{LOD}, \quad (2) \end{cases}$$

where the concentrations of a VOC ion below the limit of detection (LOD) were replaced with half of the LOD, and the associated uncertainties were set to five-sixths of the LOD using the Eq. (1). The uncertainties in a VOC ion above the LOD were calculated using the Eq. (2), assuming an error fraction of 10 %. We excluded the VOC species from the PMF analysis if their concentration data were significantly below the LOD ($> 20\%$) during the entire measurement campaign; for example, we excluded the signal of $C_4H_9^+$ from the PMF analysis because its signals were mostly below the LOD during a significant fraction of the measurement period (Fig. S4). Finally, 157 VOC ions were selected for the PMF analysis (Table S3). The sum mixing ratios of these 157 VOC ions measured by the Vocus-PTR-ToF-MS showed good agreement with the sum mixing ratios of 112 major VOC ions simultaneously measured by the CHARON-PTR-ToF-MS (Fig. S4). Therefore, the solution of the PMF analysis on these 157 VOC ions measured by the Vocus-PTR-ToF-MS can reasonably interpret the major sources and/or chemical processes of VOCs in this study. The PMF analysis was performed using the PMF Evaluation Tool (v3.05) that runs in Igor Pro software (v6.37, WaveMetrics, Portland, OR, USA). The optimal PMF solution was explored across several solution diagnostics of factors ranging from 1 to 10. The six-factor solution was chosen as the optimal and interpretable solution. After six factors, increasing the factor number will cause factor splitting and provide uninterpretable results (Fig. S5). The summary of diagnostic plots for the six-factor solution is given in Fig. S6.

2.4 Calculation of the particle-phase fraction of organic compounds

To estimate the gas-to-particle partitioning processes, we calculated the particulate mass fraction (F_p) of organic compounds using Eq. (3):

$$F_p = \frac{C_{p,i}}{C_{g,i} + C_{p,i}}, \tag{3}$$

where $C_{p,i}$ and $C_{g,i}$ are the respective particle- and gas-phase concentrations of the individual organic compound measured by CHARON-PTR-ToF-MS and Vocus-PTR-ToF-MS.

3 Results and discussion

The remainder of the text is structured as follows: in Sect. 3.1, we provide an overview of the measurements conducted; in Sect. 3.2, we address the impacts of meteorological factors, like wind speed and direction, temperature, and relative humidity on the variations in gas and particle concentrations; in Sect. 3.3, we perform a source apportionment of the VOCs observed; and, finally, in Sect. 3.4, we discuss BVOC oxidation products in the gas and particle phases.

3.1 Overview of the measurements

3.1.1 Meteorology

During the entire measurement campaign, the ambient temperature ranged from 6.8 to 30.8 °C, with an average of 16.6 ± 4.7 °C, and the relative humidity (RH) varied from 31 % to 98 %, with an average of 71 % ± 16 % (Fig. 2). The wind speeds ranged from 0 to 5.5 m s^{-1}, with an average of 1.3 ± 0.9 m s^{-1}. Wind directions varied significantly during the entire measurement period. The sampling site was potentially affected by BPP-related and/or anthropogenic emissions, depending on the wind directions (Fig. 1). The leaf area index of the Eifel Forest during our measurement period was determined to be $\sim 2.5 \pm 0.02$ m^2 m^{-2} based on the ERA5 reanalysis data. The soil moisture was measured to be 0.3 ± 0.04 m^3 m^{-3} at a station located ~ 150 m southwest of the sampling site. In addition, the spatial distribution of soil moisture in the northern Eifel Forest showed low values (< 0.3 m^3 m^{-3}) in most areas covering our sampling site (Fig. S7). Therefore, the Eifel Forest was experiencing relatively dry conditions during our measurement period.

During the entire measurement campaign, we observed two characteristic episodes, Episode 1 (00:00 UTC on 9 June to 00:00 UTC on 12 June) and Episode 2 (12:00 UTC on 23 June to 12:00 UTC on 26 June), with different meteorological conditions. During Episode 1, the daily maximum temperature remained below 20 °C for 3 consecutive measurement days. During Episode 2, the daily maximum temperature exceeded 25 °C for 3 consecutive measurement days. Therefore, we hereafter define these two episodes as
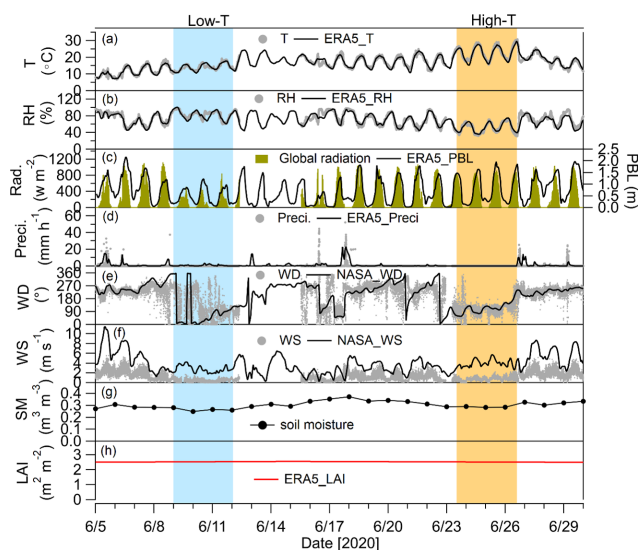
Figure 2. Time series of meteorological data measured at the sampling site and hourly **(a)** temperature (T), **(b)** relative humidity (RH), **(c)** planetary boundary layer (PBL) height and **(d)** precipitation (Preci.) data obtained from the ERA5 reanalysis (Hersbach et al., 2020) as well as hourly **(e)** wind direction (WD) and **(f)** wind speed (WS) data obtained from the NASA POWER Data Access Viewer (https://power.larc.nasa.gov/, last access: 10 October 2023). Panel **(g)** presents the daily soil moisture (SM) measured by a cosmic-ray neutron sensor, which was located ~ 150 m southwest of the sampling site, and panel **(h)** displays the leaf area index (LAI) obtained from ERA5 reanalysis. The blue and yellow shaded areas mark the low-T and high-T episodes, respectively.

low-T and high-T episodes, respectively. Both episodes had very low wind speeds (< 1 m s^{-1}), suggesting that the site was influenced by local emissions and chemical transformation or aging processes. The impacts of meteorology and chemical processes on the variations in gases and particles will be discussed in the following sections.

3.1.2 Mixing ratios of gas species

As shown in Fig. 3, the average mixing ratios of CO and CO_2 for the 10–30 June period were 0.11 ± 0.02 ppm and 410 ± 1 ppm, respectively. The mixing ratios of CH_4 ranged from 1.90 to 2.56 ppm, with an average of 1.98 ± 0.05 ppm. Spikes of CH_4 (> 2.2 ppm) were occasionally observed during the days of 17, 20–21 and 23 June and were associated with BPP-related emissions, as validated in Sect. 3.2. Isoprene and monoterpenes were quantitatively measured by the CHARON-PTR-ToF-MS and Vocus-PTR-ToF-MS with good to fair correlations ($r = 0.92$ and 0.59 for isoprene and monoterpenes, respectively). During the entire campaign, the average mixing ratio of isoprene was 0.58 ± 0.54 ppb, which is slightly higher than values previously reported in a Norway-spruce-dominated forest (0.32 ± 0.17 ppb) in central Germany (Bourtsoukidis et al., 2014) and a mixed-

conifer forest (max 0.25 ppb) comprising Norway spruce and Scots pine (*Pinus sylvestris* L.) in Sweden (Petersen et al., 2023). The level of isoprene in this study was comparable to that (~ 0.6 ppb) observed in French Landes Forest dominated by maritime pine trees (*Pinus pinaster* Aiton) during summertime (Li et al., 2020) but higher than those (0.01–0.2 ppb) reported for boreal forests in Finland dominated by Scots pine (H. Li et al., 2021; Hellén et al., 2018). The average mixing ratios of monoterpenes (2.5 ± 5.3 ppb) in this study were also higher than those reported in a Norway-spruce-dominated forest (0.50 ± 0.21 ppb) in central Germany (Bourtsoukidis et al., 2014) but lower than those observed in the French Landes Forest (~ 6 ppb) (Li et al., 2020). Relatively low mixing ratios of monoterpenes have previously been reported for boreal forests in Finland (~ 0.8 ppb) during summertime (Li et al., 2020; Mermet et al., 2021). Note that monoterpenes had a significant concentration variation in this study, which was attributed to the occurrence of monoterpene spikes (Fig. 3d). These monoterpene spikes were mainly related to the impact of BPP-related emissions, as discussed in Sect. 3.2. In this study, the average mixing ratios of sesquiterpenes measured by the CHARON-PTR-ToF-MS were 0.01 ± 0.01 ppb, a factor of 2 higher than those measured by the Vocus-PTR-ToF-MS. The average mixing ratios of sesquiterpenes were lower than those measured by a Vocus-PTR-ToF-MS in the French Landes Forest (~ 0.06 ppb) (Li et al., 2020). It should be noted that the quantification of sesquiterpenes is affected by the degree of sesquiterpene fragmentation inside the PTR-ToF-MS, which can vary significantly depending on the instrument settings (Kim et al., 2009; Kari et al., 2018). In addition, sesquiterpenes may experience wall losses inside the inlet tubing and the instrument and might, therefore, have low transmissions (Li et al., 2020). Due to a lack of a dedicated sesquiterpene calibration in this study, the quantification of sesquiterpenes measured by the PTR-ToF-MS can be regarded as the lower limit without the consideration of fragmentation.

3.1.3 Chemical composition of aerosol particles

During the entire campaign, the average mass concentrations of $PM_{2.5}$ and BC were 5.5 ± 4.7 µg m^{-3} and 0.2 ± 0.1 µg m^{-3}, respectively (Fig. S8). The aerosol particle composition – including organic aerosol (OA), nitrate and ammonium measured by the CHARON-PTR-ToF-MS and BC measured by the Aethalometer – is simultaneously available from 22 to 30 June (Fig. 4). During this period, the average OA mass concentration was 0.8 ± 0.5 µg m^{-3}, accounting for 15 ± 6 % of $PM_{2.5}$ mass. The mass fraction of CHARON-PTR-ToF-MS-measured OA in $PM_{2.5}$ was close to that of semi-volatile oxygenated organic aerosol in $PM_{2.5}$ (9 %–13 %) resolved from the PMF analysis of OA measured by an aerosol mass spectrometer (AMS) in urban and rural environments (Song et al., 2022; Huang et al., 2019). The elemental ratios of OA (O : C and H : C) measured by the
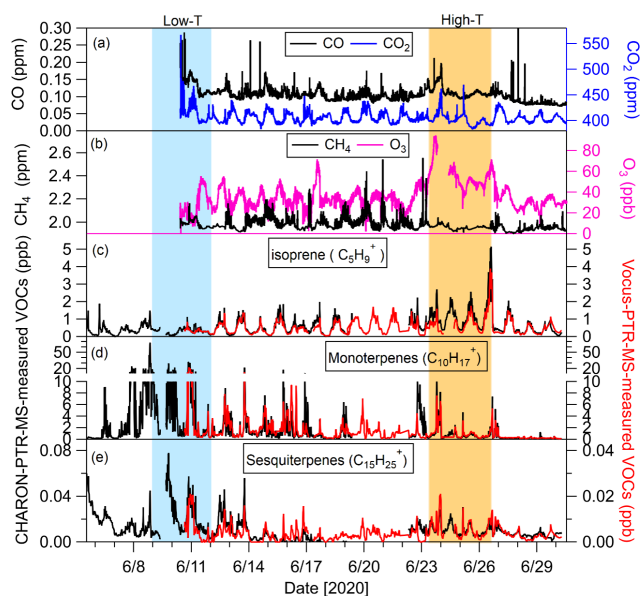
Figure 3. Time series of gas species, including **(a)** CO and CO_2; **(b)** CH_4 and O_3; and **(c)** isoprene, **(d)** monoterpenes and **(e)** sesquiterpenes measured by the CHARON-PTR-ToF-MS (black lines) and Vocus-PTR-ToF-MS (red lines). The blue and yellow shaded areas mark the low-T and high-T episodes, respectively.

Figure 4. Time series of **(a)** mass concentrations of $PM_{2.5}$, BC and semi-volatile particle species (organics, nitrate and ammonium) measured by the CHARON-PTR-ToF-MS that were simultaneously available during the 22–30 June period. Time series of the **(b)** oxygen-to-carbon (O : C) and hydrogen-to-carbon (H : C) ratios of organics. Panel **(c)** presents the average mass spectrum of organics, while panel **(d)** shows the mass distributions of organics associated with $C_xH_yO_{0-7}^+$ resolved by the carbon and oxygen numbers (n_C and n_O, respectively).

CHARON-PTR-ToF-MS were 0.32 ± 0.03 and 1.56 ± 0.10, respectively, which are comparable to the values of semi-volatile oxygenated organic aerosol (O : C of 0.35 ± 0.14 and H : C of 1.55 ± 0.10) resolved from the AMS-PMF analysis in previous studies (Ng et al., 2011, 2010). These results indicate that the OA mass detected by the CHARON-PTR-ToF-MS is mainly composed of semi-volatile organic compounds in this study. Please note that the fragmentation of organic compounds in the CHARON-PTR-ToF-MS may result in low average O : C values of bulk OA compared with those measured by the AMS (Leglise et al., 2019).

Mass concentrations of OAs associated with individual m/z signals detected by the CHARON-PTR-ToF-MS ranged from ~ 0.1 to ~ 65 ng m^{-3}. In total, 164 organic ions can be well assigned with the chemical formula of $C_xH_y^+$ or $C_xH_yO_z^+$, contributing to $67 \pm 11\%$ of total OA mass measured by the CHARON-PTR-ToF-MS. Furthermore, the organic ions assigned were mainly distributed in the C_2–C_{10} range with oxygen atom numbers of 0–5 (Fig. 4d). Müller et al. (2017) observed a similar mass distribution of OAs measured by the CHARON-PTR-ToF-MS in Valencia, Spain, which was associated with the oxidation of abundant monoterpenes emitted from trees. With the same instrument, Gkatzelis et al. (2018) also reported a similar chemical composition of OAs from the oxidation of tree emissions dominated by α-pinene and β-pinene in simulation chamber experiments. The abundant species in the C_2–C_8 range (Fig. 4d) are most likely fragments from C_{9-10}-monoterpene-derived oxidized products, which are prone

to fragmentation in the CHARON-PTR-ToF-MS (Gkatzelis et al., 2018). Leglise et al. (2019) and Peng et al. (2023) further confirm the fragmentation of oxygenated organic compounds inside the CHARON-PTR-ToF-MS via the loss of neutral water, carbonyl or carboxyl groups ($-H_2O$, $-CO$ and $-CO_2$, respectively). For instance, cis-pinonic acid ($C_{10}H_{17}O_3^+$), a monoterpene oxidation product as detected by the CHARON-PTR-ToF-MS, can produce the typical fragment ions of $C_4H_7O^+$, $C_6H_{11}O_2+$ and $C_{10}H_{15}O_2^+$ (Peng et al., 2023; Leglise et al., 2019). Furthermore, the relative abundance of fragment ions ($C_4H_7O^+$, $C_6H_{11}O_2+$ and $C_{10}H_{15}O_2^+$) was generally higher than that of the parent ion $C_{10}H_{17}O_3^+$ (Leglise et al., 2019; Peng et al., 2023). In this study, we found that only a small fraction of the cis-pinonic acid parent ion $C_{10}H_{17}O_3^+$ was detected by the CHARON-PTR-ToF-MS compared with the fragment ions $C_4H_7O^+$, $C_6H_{11}O_2^+$ and $C_{10}H_{15}O_2^+$. Similarly, other monoterpene oxidation products such as $C_9H_{15}O_3^+$ (e.g., norpinonic acid) and $C_8H_{13}O_4^+$ (e.g., norpinic acid) showed lower abundances of their parent ions compared with their fragment ions with one H_2O molecule lost ($C_9H_{13}O_2^+$ and $C_8H_{11}O_3^+$, respectively) (Fig. S9). We observed good correlations between $C_9H_{15}O_3^+$ and $C_9H_{13}O_2^+$ ($r = 0.73$) and between $C_8H_{13}O_4^+$ and $C_8H_{11}O_3^+$ (r =0.97), indicating that $C_9H_{13}O_2^+$ and $C_8H_{11}O_3^+$ are fragment ions from parent compounds. Previous studies have shown that the fragmentation pattern of oxidized organic compounds in the CHARON-PTR-ToF-MS varied depending on the instrument settings (Leglise et al.,

2019; Gkatzelis et al., 2018). Therefore, we cannot compare the fragmentation patterns of organic compounds from our instruments with those from other studies. However, it is consistent with other studies that the particulate oxidized organic compounds measured by the CHARON-PTR-ToF-MS in this study were mainly detected as the more abundant fragment ions after losing one H_2O molecule, rather than as the parent ions.

3.2 Meteorological impacts on the variations in BVOCs

We firstly analyzed the variations in the mixing ratios of gas species as a function of wind direction (WD) with a bin of 10° (Fig. 5). According to the wind and geographical conditions around the sampling site (Fig. 1b), we divided the entire measurement period into four WD sectors, including WD-forest (0–120°), WD-cut (120–240°), WD-BPP (240–300°) and WD-village (300–330°). Within the WD-forest and WD-cut sectors, the sampling site was influenced by an intact forest dominated by Norway spruce and a clear-cut area, respectively. In contrast, the sampling site was influenced by winds coming from the BPP and the village residential areas within the respective WD-BPP and WD-village sectors. We observed that the mixing ratios of CH_4 increased significantly in the WD-BPP sector along with a decrease in wind speeds and PBL heights and corresponding weaker dilution. In contrast, constantly low mixing ratios of CH_4 were observed in the WD-forest and WD-cut sectors, even when both the wind speed and PBL decreased significantly. The results indicate that the enhancement of CH_4 mixing ratios in the WD-BPP sector was mainly due to BPP emissions. In addition, CH_4 mixing ratios remained higher for the WD-village sector, which was likely associated with anthropogenic emissions from the village residential areas. We also observed a significant increase in monoterpene mixing ratios in the WD-BPP sector along with a lower ambient temperature ($\sim 15\,°C$) and decreasing radiation. This suggests that the increase in monoterpene mixing ratios in the WD-BPP sector was due to BPP emissions, rather than biogenic emissions. In contrast to CH_4, monoterpenes showed very low values in the WD-village sector, suggesting a minor contribution of anthropogenic emissions from the village residential areas to monoterpenes.

We also observed significant variations in the mixing ratios of isoprene, monoterpene and sesquiterpene in the WD-forest and WD-cut sectors, likely associated with changes in meteorological conditions, biogenic emissions and/or chemical oxidation processes. Specifically, the mixing ratios of monoterpenes and sesquiterpenes increased in the WD-forest sector (0–30°), but isoprene showed no significant change. The meteorological condition in the WD-forest sector (0–30°) was characterized by a low ambient temperature, low wind speed and shallow PBL at nighttime. Unlike isoprene, monoterpenes and sesquiterpenes can still be released from the Norway spruce in the dark (van Meeningen et al., 2017).
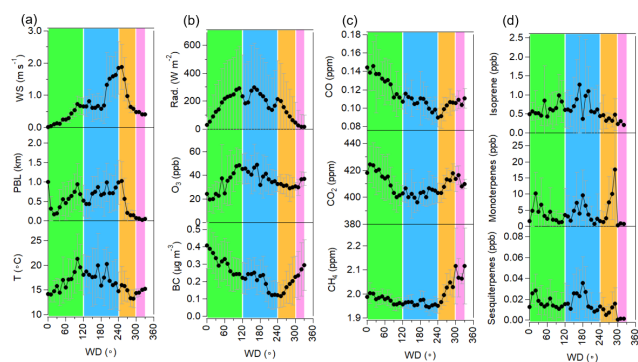
Figure 5. Variations in **(a)** wind speed (WS), planetary boundary layer (PBL) and ambient temperature; **(b)** global radiation, O_3 and BC mass concentrations; **(c)** mixing ratios of CO, CO_2 and CH_4; and **(d)** mixing ratios of isoprene, monoterpenes and sesquiterpenes as a function of wind direction (WD). The black dots and whiskers represent the respective mean values and standard deviations in each 10° WD bin. Data within the WD1 of 0–120° are influenced by an intact forest area (light green), those within the WD2 of 120–240° are influenced by a clear-cut area (light blue), those within the WD3 of 240–300° are influenced by a biogas power plant (yellow) and those within the WD4 of 300–330° are influenced by a village (pink).

Monoterpenes and sesquiterpenes could accumulate during nighttime in the WD-forest sector (0–30°) as a result of low concentrations of atmospheric oxidants like O_3. Moreover, we observed an increase in the isoprene mixing ratios in the WD-forest sector (60–120°) which coincided with increases in the wind speed, PBL, ambient temperature and radiation during daytime. In contrast, monoterpenes and sesquiterpenes showed low mixing ratios in the WD-forest sector (60–120°). It is expected that higher temperature and radiation enhanced biogenic emissions, resulting in the increase in the isoprene mixing ratios. However, lower mixing ratios of monoterpenes and sesquiterpenes were likely attributed to photochemical oxidation exceeding their biogenic emissions. The strong photochemical oxidation processes were characterized by higher radiation and O_3 mixing ratios in the WD-forest sector (60–120°). In the WD-cut sector (120–180°), we observed a simultaneous increase in isoprene, monoterpenes and sesquiterpenes, which was associated with enhanced biogenic emissions induced by a higher temperature. Conversely, a simultaneous decrease in isoprene, monoterpene and sesquiterpene mixing ratios was observed in the WD-cut sector (180–240°) along with a high ambient temperature. Note that the sampling site was more influenced by the distant Norway Spruce trees in the WD-cut sector (120–180°) compared with the WD-cut sector (180–240°) (Fig. 1a). In addition, the wind speeds were significantly higher in the WD-cut sector (180–240°). Therefore, the decreases in isoprene, monoterpene and sesquiterpene mixing ratios in the WD-cut sector (180–240°) were attributed to the reduced biogenic emissions of fewer Norway spruce and the

dilution effect caused by higher wind speeds. The dilution effect was supported by the lowest CO mixing ratios and BC mass concentrations observed in the WD-cut sector (180–240°).

Based on the above WD analyses, we further investigated the diurnal variations in meteorological parameters as well as gas species in two major groups influenced by anthropogenic (WD-BPP and WD-village) and biogenic (WD-forest and WD-cut) emissions, respectively (Fig. 6). In the anthropogenic group, the diurnal variations in CH_4 mixing ratios showed higher values during nighttime, which were related to BPP emissions and a low wind speed and PBL height. However, a less pronounced diurnal variation in CH_4 mixing ratios was observed under the influence of biogenic emissions (biogenic group). In the anthropogenic group, the diurnal behavior of monoterpenes showed higher mixing ratios during nighttime, although with large fluctuations over the whole day. These fluctuations with monoterpene spikes were related to BPP emissions, depending on the wind directions. As expected, isoprene showed higher mixing ratios during daytime in the biogenic group, which is similar to the diurnal behavior of the isoprene emission rate in previous observations in Norway-spruce-dominated forests (Bourtsoukidis et al., 2014; Juráò et al., 2017). However, in the biogenic group, the diurnal variations in monoterpenes and sesquiterpenes showed very low mixing ratios during daytime due to the higher PBL and strong photochemical consumption. The concentrations of monoterpenes and sesquiterpenes peaked at ∼ 18:00 UTC, at which time the concentrations of atmospheric oxidants (OH radicals and O_3) and the PBL heights decreased. Monoterpenes and sesquiterpenes showed low mixing ratios of < 1 and < 0.01 ppb, respectively, after 18:00 UTC (during nighttime) in the biogenic group. This is different from previous studies in boreal forests that have reported constantly higher mixing ratios of monoterpenes and sesquiterpenes but lower O_3 values (< 20 ppb) during nighttime (Hakola et al., 2012; Li et al., 2020). However, in our study, higher O_3 mixing ratios (∼ 30 ppb) were observed during nighttime in the biogenic group, which may have reduced the concentrations of monoterpenes and sesquiterpenes via nighttime oxidation. Note that the mixing ratios of monoterpenes and sesquiterpenes were low during daytime, but they increased slightly from 08:00 to 12:00 UTC when the temperature and radiation increased. Figure 7 shows the time series of isoprene, monoterpenes, sesquiterpenes and O_3 along with the wind direction, ambient temperature and radiation during low-T and high-T episodes. During daytime in the high-T episode, we observed that the mixing ratios of isoprene, monoterpenes and sesquiterpenes all increased as the temperature increased when the sampling site was constantly influenced by a ∼ 100° WD from the intact forest. Meanwhile, higher radiation and constantly high mixing ratios of O_3 (40–60 ppb) were observed during daytime in the high-T episode. The photochemical O_3 production is also supported
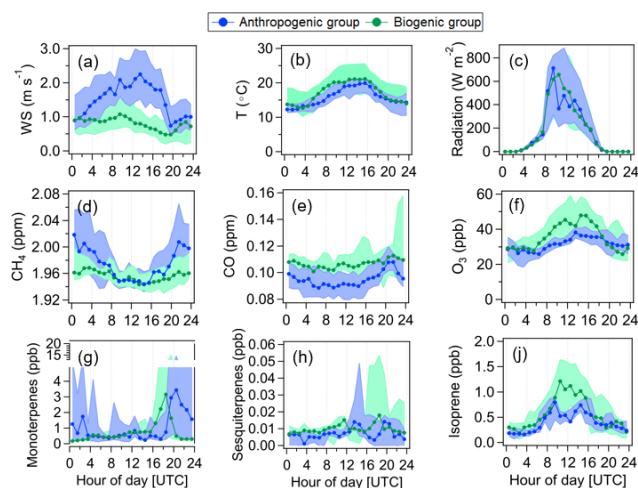
Figure 6. Diurnal variations in **(a)** wind speed, **(b)** ambient temperature and **(c)** global radiation; **(d)** CH_4, **(e)** CO and **(f)** O_3; and **(g)** monoterpenes, **(h)** sesquiterpenes and **(i)** isoprene. The blue and green markers represent the median values for the anthropogenic group and biogenic group that were calculated from the data within the WD-forest and WD-cut sectors and the WD-BPP and WD-village sectors, respectively. The shaded areas represent the 25th and 75th percentiles.

by higher BVOC mixing ratios. However, the increasing biogenic emissions due to higher temperatures and solar radiation obviously exceeded the photochemical consumption. Similarly, higher mixing ratios of O_3 were observed during daytime in the low-T episode, during which time the sampling site was also constantly influenced by a ∼ 100° wind direction (e.g., 11 June). However, the mixing ratios of isoprene, monoterpenes and sesquiterpenes showed no increase. In Fig. 7a, we also see that very high mixing ratios of monoterpenes and sesquiterpenes during the low-T episode (e.g., 20:00–24:00 UTC on 10 June) were associated with changes in wind directions, which is in line with the WD analyses (as discussed above). Furthermore, soil moisture showed no significant difference between the low-T and high-T episodes (Fig. 2). We cannot demonstrate the impact of soil moisture on the variations in BVOC mixing ratios due to the fact that the observation period used in this study was short.

3.3 Source apportionment of VOCs

In addition to meteorological impacts, the variations in VOC concentrations are influenced by different emission sources and chemical processes. We performed a PMF analysis of Vocus-PTR-ToF-MS-measured VOC data to identify and determine the impacts of different sources and oxidation processes. According to the factor profiles and temporal variations, we present a six-factor solution, including one terpene-dominated factor, one factor related to BVOC oxidation during nighttime, one factor related to aromatic VOC oxidation
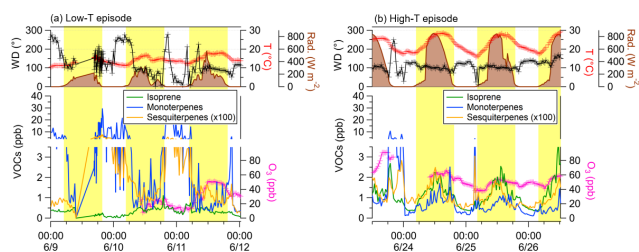
Figure 7. Time series of wind direction, ambient temperature, global radiation, isoprene, monoterpenes, sesquiterpenes and O_3 during the low-T episode **(a)** and high-T episode **(b)**. The yellow shaded areas mark daytime (from 04:00 to 20:00 UTC).

and three factors related to daytime BVOC oxidation. Figure 8 shows the factor profiles, time series and diurnal variations in the six factors as well as their relative contribution to total VOCs (TVOCs) during the entire measurement campaign.

The first factor profile was dominated by the monoterpene parent ion ($C_{10}H_{17}^+$) and its fragment ion ($C_6H_9^+$) (Tani et al., 2003; Kari et al., 2018). Furthermore, this factor was characterized by a higher fraction of monoterpenoids, such as $C_{10}H_{17}O^+$ (camphor or monoterpene oxide) and $C_{10}H_{19}O^+$ (linalool or monoterpene water cluster), in the high-mass range (m/z 140–230) (Li et al., 2020). These monoterpenoids can be emitted by leaves and flowers directly (Joó et al., 2010); therefore, we define this factor as a terpene-dominated factor. As discussed before, the variations in monoterpene concentrations were influenced by the BPP emissions and biogenic emissions, depending on the wind direction. In this study, PMF analysis could not separate the relative contribution of biogenic emissions and BPP emissions to monoterpenes directly. This is probably due to the source profile of BPP emissions dominated by the monoterpenes, which is similar to that of biogenic emissions. Based on the WD analyses, this factor was expected to be mainly associated with the biogenic emissions when the winds were coming from the forest. In contrast, when the winds were coming from the BPP, this factor was significantly contributed by the BPP emissions.

The second factor profile was characterized by high fractions of $C_{10}H_{17}O^+$ (monoterpene oxide), $C_{10}H_{17}O_2^+$ and $C_{10}H_{15}O^+$ (pinonaldehyde and its fragment ion) in the high-mass range. These compounds were weakly oxidized products of monoterpenes with an oxygen atom number < 3, as found by previous studies (H. Li et al., 2021; Li et al., 2020; Vermeuel et al., 2023). In addition, this factor was dominated by $C_3H_7O^+$ (acetone), which could be contributed by the primary emissions and the oxidation of VOCs from both biogenic and anthropogenic sources (Jacob et al., 2002). The diurnal pattern of the second factor showed higher concentrations at nighttime. Therefore, we define this factor as representing the secondary oxidation processes of BVOCs, especially monoterpenes, during nighttime (night-SecVOC).
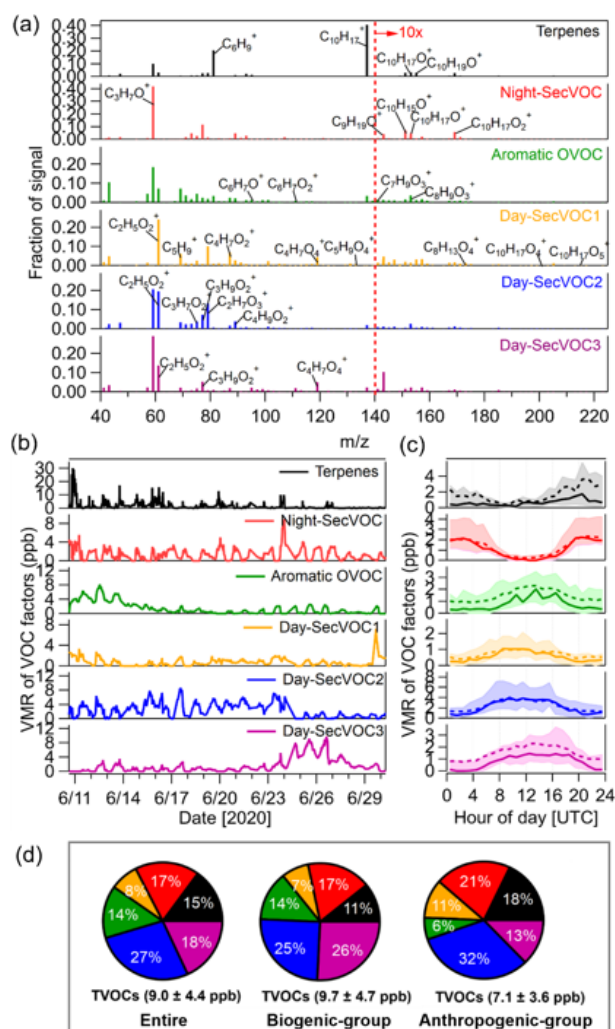
Figure 8. Panel **(a)** presents factor profiles of the six VOC factors resolved from the PMF analysis of Vocus-PTR-ToF-MS data. The fraction of signal in the high-mass range (m/z 140–230) is scaled by a factor of 10. Panel **(b)** shows time series of the six VOC factors. Panel **(c)** displays diurnal variations in the six VOC factors during the entire measurement campaign. The solid and dashed lines represent median and mean values, respectively, and the shaded areas represent the 25th and 75th percentiles. Panel **(d)** outlines the average contributions of the six VOC factors to TVOCs for the entire measurement campaign and for the separate biogenic and anthropogenic groups.

H. Li et al. (2021) performed a binPMF analysis on Vocus-PTR-ToF-MS-measured VOC data at two European forest sites. They also resolved a factor representing weakly oxidized products of monoterpenes with higher concentrations at night (H. Li et al., 2021).

The third factor profile was characterized by higher fractions of $C_6H_7O^+$ (phenol), $C_6H_7O_2^+$ (catechol) and $C_7H_7O_2^+$ (benzoic acid) compared with other factors. Furthermore, this factor was dominated by $C_7H_9O_3^+$ (e.g., oxo-heptedienoic acid) and $C_8H_9O_3^+$ (e.g., vanillin) in the high-

mass range. These OVOC species could have originated from the oxidation of aromatic hydrocarbons (Hamilton et al., 2005; Zaytsev et al., 2019; Y. Li et al., 2021; Wu et al., 2014; Lannuque et al., 2023). As expected, good correlations were found for aromatic OVOC with catechol ($r = 0.87$ for $C_6H_7O_2^+$) and benzoic acid ($r = 0.84$ for $C_7H_7O_2^+$). In addition, this factor also correlated well ($r = 0.77$–0.87; Fig. S10) with $C_5H_5O_3^+$ (e.g., methylfurandione), $C_5H_5O_2^+$ (e.g., butenedial), $C_4H_5O_2^+$ (e.g., furfural) and $C_3H_5O_2^+$ (e.g., methylglyoxal). These compounds are likely ring-opening products of toluene oxidation, as reported in previous studies (Zaytsev et al., 2019; Wu et al., 2014; Lannuque et al., 2023). Therefore, we identified this factor as a factor of aromatic OVOC representing the OVOCs formed from the oxidation of aromatic hydrocarbons. The diurnal variation in the aromatic OVOC factor showed slightly higher concentrations during daytime, which can be related to an enhanced photochemical oxidation of aromatic hydrocarbons.

In this study, we also resolved three factors related to the oxidation of BVOCs during daytime, denoted as day-SecVOC1, day-SecVOC2 and day-SecVOC3. The factor profile of day-SecVOC1 was characterized by high fractions of acetic acid ($C_2H_5O_2^+$) as well as isoprene and its oxidation products (e.g., $C_5H_9^+$, $C_4H_7O_{1-4}^+$ and $C_5H_9O_{2-4}^+$). This factor was also dominated by stronger oxidized products of monoterpenes with oxygen atom numbers > 3 (e.g., $C_{10}H_{17}O_{4-5}^+$) compared with other factors in the higher-mass range. The diurnal variations in the day-SecVOC1 factor showed high concentrations during daytime. Therefore, the day-SecVOC1 factor can be mainly attributed to the photochemical oxidation of isoprene and monoterpenes during daytime. H. Li et al. (2021) resolved one factor representing isoprene and its oxidation products and another factor representing stronger oxidized products of monoterpenes from the binPMF analysis for a low-mass (m/z 50–200) and a high-mass (m/z 201–320) range, respectively, for two European forest sites. They found that these two factors had a similar diurnal pattern with high daytime concentrations. In our study, we performed the PMF analysis for the full mass range (m/z 40–230) of the major VOC ions and resolved the day-SecVOC1 factor containing high fractions of oxidized products of isoprene and monoterpenes. This suggests that isoprene oxidation products and more highly oxidized products of monoterpenes were mainly related to the daytime oxidation processes. The factor profiles of both day-SecVOC2 and day-SecVOC3 were characterized by high fractions of acetone ($C_3H_7O^+$) and acetic acid ($C_2H_5O_2^+$). Acetone and acetic acid could be contributed by biogenic and anthropogenic secondary sources (Khare et al., 1999; Jacob et al., 2002). The factor profile of day-SecVOC2 also had high fractions of $C_2H_7O_3^+$ (acetic acid water cluster), $C_3H_7O_2^+$ (propionic acid), $C_4H_9O_2^+$ (butyric acid) and $C_3H_9O_2^+$ (e.g., propylene glycol). These gaseous organic acids could be formed from the oxidation of BVOCs like monoterpenes (Friedman and Farmer, 2018). In addition,

the factor profile of day-SecVOC3 showed higher fractions of $C_4H_7O_4^+$ (e.g., succinic acid) compared with other factors. The time series of day-SecVOC3 showed the highest correlations with $C_2H_7O_3^+$ (acetic acid water cluster, $r = 0.79$), $C_2H_5O_2^+$ (acetic acid, $r = 0.63$) and $C_3H_9O_3^+$ (propionic acid water cluster) compared with other factors. The time series of the day-SecVOC3 factor also showed strong correlations with $C_4H_6O^+$ ($r = 0.90$, Fig. S10) and $C_2H_5O_3^+$ ($r = 0.89$), which can be assigned to the isoprene oxidation product as deprotonated $C_4H_7O^+$ (methyl vinyl ketone, MVK, and methacrolein, MACR) and glycolic acid, respectively. In addition, O_3 was only weakly correlated with day-SecVOC2 ($r = 0.27$) but was much more highly correlated with day-SecVOC3 ($r = 0.57$). Moreover, a better correlation was found between O_3 and the sum of these two factors ($r = 0.70$). The diurnal variations in both factors showed higher concentrations during daytime. Based on these results, we identified day-SecVOC2 and day-SecVOC3 as representing low-molecular-weight oxygenated organic compounds produced from the daytime photooxidation of BVOCs.

As shown in Fig. 8, the mixing ratios of TVOCs measured by the Vocus-PTR-ToF-MS for the PMF analysis were 9.0 ± 4.4 ppb during the entire campaign. The mixing ratios of TVOCs were dominated by the daytime BVOC oxidation, with day-SecVOC1 ($8\% \pm 5\%$), day-SecVOC2 ($27\% \pm 20\%$) and day-SecVOC3 ($18\% \pm 21\%$). This indicates substantial contributions of oxygenated species to TVOCs during the entire campaign. Based on the WD analysis, we further compared the relative contributions of VOC factors to TVOCs for the groups influenced by the respective biogenic and anthropogenic emissions. The average mixing ratios of TVOCs in the biogenic group (9.7 ± 4.7 ppb) were slightly higher than those in the anthropogenic group (7.1 ± 3.6 ppb). The contribution of day-SecVOC2 to TVOCs was comparable, with $25\% \pm 21\%$ and $32\% \pm 18\%$ for the biogenic and anthropogenic groups, respectively. However, the contribution of day-SecVOC3 to TVOCs in the biogenic group ($26\% \pm 25\%$) was higher than that in the anthropogenic group ($13\% \pm 15\%$). We observed significantly elevated mixing ratios of isoprene (Fig. 3c) and day-SecVOC3 during the high-T episode (Fig. 8). As mentioned before, the sampling site was mainly influenced by the winds coming from the intact forest during the high-T episode, along with higher mixing ratios of O_3. Therefore, the higher contribution of day-SecVOC3 in the biogenic group was attributed to the strong oxidation of BVOCs, especially of isoprene. The contribution of the terpene-dominated factor to TVOCs was higher in the anthropogenic group ($18\% \pm 16\%$) compared with that in the biogenic group ($11\% \pm 15\%$). This is consistent with the WD analyses, in which higher monoterpene mixing ratios were related to the BPP emissions. In addition, the contributions of the night-SecVOC and day-SecVOC1 factors to the TVOC concentrations were slightly higher in the anthropogenic group; this was related to the high abundances of monoterpenes. Further-

more, gas-to-particle partitioning processes could also have influenced the variations in BVOC oxidation products and, thus, the night-SecVOC and day-SecVOC1 factors.

3.4 Variations in BVOC oxidation products in the gas and particle phases

Figure 9 shows the diurnal variations in the concentrations of organic molecules ($C_5H_9O_{1-4}^+$, $C_4H_7O_{1-4}^+$, $C_{10}H_{17}O_{1-5}^+$ and $C_{10}H_{15}O_{1-5}^+$) in the gas phase measured by the Vocus-PTR-ToF-MS and in particle-phase compounds measured by the CHARON-PTR-ToF-MS during the 22–30 June period. These organic molecules are important components of the night-SecVOC and day-SecVOC1 factors resolved by the PMF analysis, and they are identified as the oxidation products from isoprene and monoterpenes based on previous field observations and simulation chamber experiments (Gkatzelis et al., 2018; Li et al., 2020). For example, gaseous $C_4H_7O^+$ can be the sum of MVK and MACR, which are major products of isoprene oxidation (Wennberg et al., 2018). $C_{10}H_{17}O_3^+$ can be attributed to *cis*-pinonic acid formed from the oxidation of monoterpenes (e.g., α-pinene). Again, the fragmentation of high-molecular weight oxidized organic compounds measured by the PTR-ToF-MS instruments could produce fragment ions via the loss of neutral water, carbonyl or carboxyl groups (–H_2O, –CO and –CO_2, respectively). The diurnal variations in all isoprene oxidation products ($C_5H_9O_{1-4}^+$ and $C_4H_7O_{1-4}^+$) in both the gas and particle phases showed higher concentrations from morning (06:00–08:00 UTC) to afternoon (12:00–16:00 UTC), as did isoprene itself. These results indicate that higher temperatures and intensive sunlight not only favor isoprene emissions but also enhance the photochemical oxidation of isoprene. Moreover, we found that the concentrations of particulate $C_4H_7O_{1-2}^+$ showed increased values from evening (18:00–20:00 UTC) to around midnight (00:00–02:00 UTC of the next day). As mentioned before, the fragmentation of *cis*-pinonic acid in the CHARON-PTR-ToF-MS can produce the fragment ions $C_4H_7O^+$, $C_6H_{11}O_2+$ and $C_{10}H_{15}O_2^+$ (Gkatzelis et al., 2018; Peng et al., 2023; Müller et al., 2017; Leglise et al., 2019). Furthermore, we observed a similar diurnal pattern of $C_4H_7O^+$ and $C_{10}H_{15}O_2^+$ in the particle phase, suggesting that the nighttime increase in the particulate $C_4H_7O^+$ was likely contributed by the fragmentation of *cis*-pinonic acid. Due to instrumental limitations, it is difficult to assign each ion detected by the PTR-ToF-MS to either a parent ion or a fragment ion of one organic compound in the ambient particles.

The diurnal variations in the weakly oxidized products of monoterpenes, like $C_{10}H_{17}O_{1-2}^+$ and $C_{10}H_{15}O_{1-2}^+$, in both the gas and particle phases showed elevated concentrations during nighttime. In contrast, the more-oxidized products of monoterpenes ($C_{10}H_{17}O_{4-5}^+$ and $C_{10}H_{15}O_{4-5}^+$) showed higher concentrations in the gas and particle phases during daytime. The higher atmospheric oxidation capacity dur-
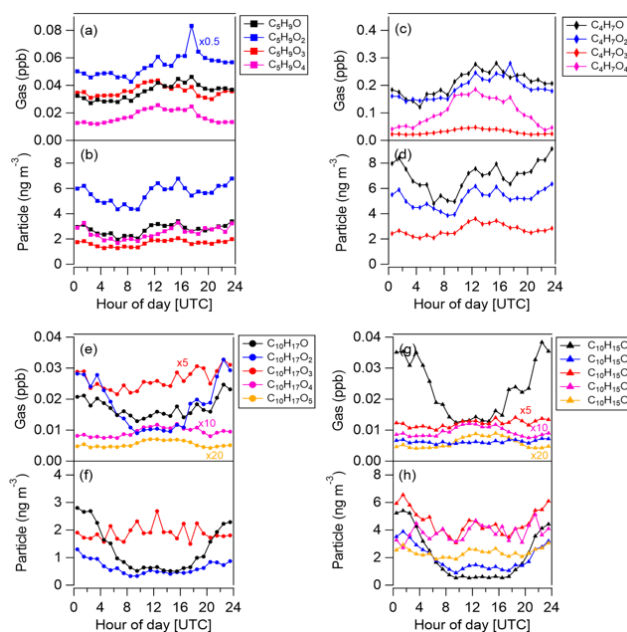
Figure 9. Diurnal variations in (**a–d**) isoprene oxidation products ($C_5H_9O_{1-4}^+$ and $C_4H_7O_{1-4}^+$) in the gas and particle phases and in (**e–h**) monoterpene oxidation products ($C_{10}H_{17}O_{1-5}^+$ and $C_{10}H_{15}O_{1-5}^+$) in the gas and particle phases calculated for the measurement period from 22 to 30 June. Gas- and particle-phase data were taken from the Vocus-PTR-ToF-MS and CHARON-PTR-ToF-MS measurements, respectively. The more highly oxidized particle-phase products from isoprene ($C_4H_7O_4^+$) and monoterpenes ($C_{10}H_{17}O_{4-5}^+$) cannot be detected by the CHARON-PTR-ToF-MS.

ing daytime compared with nighttime leads to the formation of more-oxidized products. In addition, $C_{10}H_{17}O_3^+$ (*cis*-pinonic acid) and its fragment ion ($C_{10}H_{15}O_2^+$) in the gas phase showed less pronounced diurnal patterns. The particulate $C_{10}H_{17}O_3^+$ also showed a less pronounced diurnal behavior, while the particulate $C_{10}H_{15}O_2^+$ showed increased concentrations during nighttime. This is in agreement with previous findings in that most of the particulate compounds detected by the CHARON-PTR-ToF-MS were not detected as the parent ion, rather as the fragment ion with one H_2O molecule lost (Gkatzelis et al., 2018). In this study, $C_{14}H_{23}O_2^+$, $C_{15}H_{23}O^+$ and $C_{15}H_{25}O_2^+$ were measured by the PTR instruments and can be considered to be sesquiterpene oxidation products based on previous field and simulation chamber studies. Here, $C_{14}H_{23}O_2^+$ was only detected in the gas phase by the Vocus-PTR-ToF-MS, while $C_{15}H_{23}O_2^+$ and $C_{15}H_{25}O_2^+$ were only detected in the particle phase by the CHARON-PTR-ToF-MS. The concentrations of sesquiterpene oxidation products in both the gas (< 0.5 ppt) and particle (< 5 ng m^{-3}) phases were relatively low, likely due to correspondingly low concentrations of sesquiterpenes in this study. The diurnal pattern of gaseous $C_{14}H_{23}O_2^+$ showed two peaks, one in the morning and one in the early evening
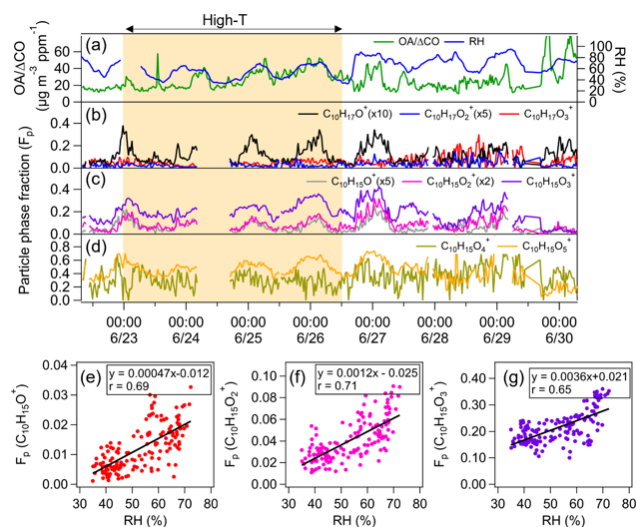
Figure 10. Time series of **(a)** OA/ΔCO and relative humidity (RH) and of **(b–d)** the particle-phase fraction of monoterpene oxidation products ($C_{10}H_{17}O_{1-3}^+$ and $C_{10}H_{15}O_{1-5}^+$) from 22 to 30 June. The yellow shaded area marks the high-T episode. **(e–f)** Correlations of the time series of the particle-phase fraction of $C_{10}H_{15}O_{1-3}^+$ with RH during the high-T episode.

(Fig. S11), similar to those of weakly oxidized products of sesquiterpenes (e.g., $C_{14}H_{22}O_{1-3}$ and $C_{15}H_{24}O_{1-3}$) observed at the Landes Forest in France (Li et al., 2020). The diurnal variations in the particulate $C_{15}H_{23}O_2^+$ and $C_{15}H_{25}O_2^+$ showed slightly higher values during nighttime.

Furthermore, we calculated the variations in OA/ΔCO, which represents the total OA concentrations measured by the CHARON-PTR-ToF-MS normalized over ΔCO (the background CO concentration is subtracted) during the 22–30 June period (Fig. 10). CO is relatively long-lived; thus, normalizing the observed OA mass concentrations to the background-corrected CO helps to minimize the impacts of boundary layer dynamics (De Gouw and Jimenez, 2009). An increase in OA/ΔCO was observed during nighttime in the high-T episode, which could be related to the gas-to-particle partitioning of BVOC oxidation products. Based on the two PTR measurements, we calculated the particulate fraction of representative monoterpene oxidation products (i.e., $C_{10}H_{17}O_{1-3}^+$ and $C_{10}H_{15}O_{1-5}^+$) to estimate their gas-to-particle partitioning processes. The two PTR instruments used in this study may have different sensitivities or fragmentation for different oxygenated organic compounds. For example, the concentrations of monoterpene oxidation products, such as $C_9H_{15}O^+$, $C_{10}H_{15}O_{1-2}^+$ and $C_{10}H_{17}^+$, measured by the Vocus-PTR-ToF-MS were $\sim$ 2–3 times higher than those measured by the CHARON-PTR-ToF-MS (Fig. S13b). Although we cannot precisely calculate the F_p values for each OA molecule due to instrumental limitations, the variations in the calculated F_p values can still be used as an indicator to estimate the gas-to-particle portioning processes.

As shown in Fig. 10, weakly oxidized molecules of monoterpenes ($C_{10}H_{17}O_{1-2}^+$ and $C_{10}H_{15}O_{1-3}^+$) had lower F_p values compared with more-oxidized molecules of monoterpenes ($C_{10}H_{17}O_3^+$ and $C_{10}H_{15}O_{4-5}^+$). This is expected, as more-oxidized products of monoterpenes generally have lower volatility compared with weakly oxidized ones. Interestingly, the F_p values of weakly oxidized molecules of monoterpenes showed similar temporal trends to the relative humidity. Especially for the high-T episode, the F_p values of weakly oxidized molecules of monoterpenes ($C_{10}H_{15}O_{1-3}^+$) showed positive correlations ($r = 0.65$–0.71) with RH. This indicates that increasing RH can enhance the particle fraction of weakly oxidized molecules of monoterpenes and, thus, increase the SOA mass. As validated in Sect. 3.3, these weakly oxidized molecules of monoterpenes are formed by the oxidation of monoterpenes emitted from trees during the high-T episode, rather than from BPP emissions. It is reasonable to assume that these monoterpenes are mainly α-pinene and β-pinene, as our sampling site was in a forest dominated by Norway spruce, which is known to emit mainly pinenes (Christensen et al., 2000; Hakola et al., 2017). Previously, Tillmann et al. (2010) found that the SOA yields from the ozonolysis of α-pinene were higher under humid conditions than under dry conditions. More recently, Surdu et al. (2023) studied the effect of RH on the partitioning of oxidized organic molecules formed from α-pinene oxidation at the CERN Cosmics Leaving Outdoor Droplets (CLOUD) chamber. They observed that the particle-phase concentrations of semi-volatile organic molecules ($C_{10}H_{16}O_{2-3}$) from α-pinene oxidation significantly increase (by factors of 2–4) with increasing RH, leading to a substantial increase in the SOA mass (Surdu et al., 2023). Similarly, Luo et al. (2024) reported that increasing the RH from 3 % to 84 % increases the abundance of less-oxidized products (e.g., $C_{10}H_{16}O_{2-6}$) from α-pinene ozonolysis. In our study, during the high-T episode, we observed that the F_p values for $C_{10}H_{15}O^+$, $C_{10}H_{15}O_2^+$ and $C_{10}H_{15}O_3^+$ increased by $\sim$ 2 %, $\sim$ 6 % and $\sim$ 20 %, respectively, when RH was increased from 30 %–40 % to 60 %–80 %. Furthermore, the ambient temperature was anticorrelated with RH in this study. Thus, lower temperatures may also further favor the gas-to-particle partitioning of semi-volatile organic molecules from monoterpene oxidation.

4 Conclusions

In this study, we investigated the characteristics of VOCs and OA particles simultaneously measured by a CHARON-PTR-ToF-MS and a Vocus-PTR-ToF-MS at a Norway-spruce-dominated forest stressed by bark beetles and droughts close to a BPP in western Germany during June 2020. The average mass concentration of OA particles detected by the CHARON-PTR-ToF-MS was $0.8 \pm 0.5\ \mu g\,m^{-3}$. The chemical composition of OA ions ranged between C_2 and C_{10}

with oxygen atom numbers of 0–5, which were mainly attributed to the semi-volatile organic compounds formed from monoterpene oxidation. The average mixing ratios of isoprene and monoterpenes were higher than the values previously measured in both German temperate forests and boreal forests during summertime (Mermet et al., 2021; H. Li et al., 2021; Hellén et al., 2018; Bourtsoukidis et al., 2014); this may be due to the effect of environmental stressors, such as long-lasting droughts and bark beetle infestation, and differences in the meteorological conditions. Based on the WD analyses, BVOC data were categorized into two groups to distinguish the impacts of biogenic emissions from an intact forest and a clear-cut area (biogenic group) and anthropogenic emissions from a BPP and a village (anthropogenic group). The mixing ratios of CH_4 and monoterpenes showed significantly higher values in the anthropogenic group. This was expected for CH_4, and it is also known that BPP can release high concentrations of monoterpenes during biowaste storage and fermentation processes (Salazar Gómez et al., 2016; Papurello et al., 2012). In the biogenic group, the variations in mixing ratios of isoprene, monoterpenes and sesquiterpenes were driven by the interplay between meteorological conditions, biogenic emissions and subsequent chemical oxidation processes. Based on the PMF analysis of VOCs measured by the Vocus-PTR-ToF-MS, six factors were resolved, representing the major sources and/or products of chemical transformation processes. During the entire measurement period, TVOCs were largely composed of oxygenated organic compounds formed from the photochemical oxidation of BVOCs during daytime. However, monoterpenes and their weakly oxidized products (e.g., $C_{10}H_{15}O_{1-3}^+$ and $C_{10}H_{17}O_{1-2}^+$) dominated the TVOCs during nighttime. These weakly oxidized monoterpene products in the particle phase also showed higher concentrations during nighttime. In contrast, more-oxidized monoterpene products (e.g., $C_{10}H_{17}O_{4-5}^+$ and $C_{10}H_{15}O_{4-5}^+$) in both the gas and particle phases were more abundant during daytime. By combining the gas and particle data measured by the CHARON-PTR-ToF-MS and the Vocus-PTR-ToF-MS, we found that increasing RH and decreasing temperature led to an increase in the particulate fraction of weakly oxidized monoterpene products, consistent with the findings from recent simulation chamber studies (Surdu et al., 2023; Luo et al., 2024). Overall, this study demonstrates that the variations in BVOCs in a typical stressed European coniferous forest are influenced not only by meteorology and biogenic emissions but also by local anthropogenic emissions (e.g., from a BPP) and subsequent chemical transformation processes. The impact of soil moisture, tree species composition and tree health conditions on the variations in BVOC concentrations could not be fully addressed due to the relative short observation period. Thus, future long-term field measurements, including seasonality and detailed tree characterization, are necessary to assess the impacts of droughts and bark beetle outbreaks on BVOC emissions and the subsequent formation of SOA.

Author contributions. JS, HS and RT conducted the field measurements; JS and GG carried out the CHARON-PTR-ToF-MS and Vocus-PTR-ToF-MS data analysis, respectively; NB and TL provided general comments on this paper; and JS drafted the manuscript with contributions from all co-authors.

References

Atkinson, R.: Atmospheric chemistry of VOCs and NO$_x$, Atmos. Environ., 34, 2063–2101, https://doi.org/10.1016/S1352-2310(99)00460-4, 2000.

Bakkaloglu, S., Lowry, D., Fisher, R. E., France, J. L., Brunner, D., Chen, H., and Nisbet, E. G.: Quantification of methane emissions from UK biogas plants, Waste Manag., 124, 82–93, https://doi.org/10.1016/j.wasman.2021.01.011, 2021.

Bogena, H. R., Huisman, J. A., Güntner, A., Hübner, C., Kusche, J., Jonard, F., Vey, S., and Vereecken, H.: Emerging methods for noninvasive sensing of soil moisture dynamics from field to catchment scale: a review, WIREs Water, 2, 635–647, https://doi.org/10.1002/wat2.1097, 2015.

Bonn, B., Magh, R.-K., Rombach, J., and Kreuzwieser, J.: Biogenic isoprenoid emissions under drought stress: different responses for isoprene and terpenes, Biogeosciences, 16, 4627–4645, https://doi.org/10.5194/bg-16-4627-2019, 2019.

Bourtsoukidis, E., Williams, J., Kesselmeier, J., Jacobi, S., and Bonn, B.: From emissions to ambient mixing ratios: online seasonal field measurements of volatile organic compounds over a Norway spruce-dominated forest in central Germany, Atmos. Chem. Phys., 14, 6495–6510, https://doi.org/10.5194/acp-14-6495-2014, 2014.

Bourtsoukidis, E., Pozzer, A., Williams, J., Makowski, D., Peñuelas, J., Matthaios, V. N., Lazoglou, G., Yañez-Serrano, A. M., Lelieveld, J., Ciais, P., Vrekoussis, M., Daskalakis, N., and Sciare, J.: High temperature sensitivity of monoterpene emissions from global vegetation, Commun. Earth Environ., 5, 23, https://doi.org/10.1038/s43247-023-01175-9, 2024.

Brémond, U., Bertrandias, A., Steyer, J.-P., Bernet, N., and Carrere, H.: A vision of European biogas sector development towards 2030: Trends and challenges, J. Clean. Prod., 287, 125065, https://doi.org/10.1016/j.jclepro.2020.125065, 2021.

Byron, J., Kreuzwieser, J., Purser, G., van Haren, J., Ladd, S. N., Meredith, L. K., Werner, C., and Williams, J.: Chiral monoterpenes reveal forest emission mechanisms and drought responses, Nature, 609, 307–312, https://doi.org/10.1038/s41586-022-05020-5, 2022.

Christensen, C. S., Hummelshøj, P., Jensen, N. O., Larsen, B., Lohse, C., Pilegaard, K., and Skov, H.: Determination of the terpene flux from orange species and Norway spruce by relaxed eddy accumulation, Atmos. Environ., 34, 3057–3067, https://doi.org/10.1016/S1352-2310(99)00502-6, 2000.

De Gouw, J. and Jimenez, J. L.: Organic Aerosols in the Earth's Atmosphere, Environ. Sci. Technol., 43, 7614–7618, https://doi.org/10.1021/es9006004, 2009.

Desservettaz, M., Pikridas, M., Stavroulas, I., Bougiatioti, A., Liakakou, E., Hatzianastassiou, N., Sciare, J., Mihalopoulos, N., and Bourtsoukidis, E.: Emission of volatile organic compounds from residential biomass burning and their rapid chemical transformations, Sci. Total Environ., 903, 166592, https://doi.org/10.1016/j.scitotenv.2023.166592, 2023.

Eichler, P., Müller, M., D'Anna, B., and Wisthaler, A.: A novel inlet system for online chemical analysis of semi-volatile submicron particulate matter, Atmos. Meas. Tech., 8, 1353–1360, https://doi.org/10.5194/amt-8-1353-2015, 2015.

Faiola, C. and Taipale, D.: Impact of insect herbivory on plant stress volatile emissions from trees: A synthesis of quantitative measurements and recommendations for future research, Atmos. Environ.-X, 5, 100060, https://doi.org/10.1016/j.aeaoa.2019.100060, 2020.

Friedman, B. and Farmer, D. K.: SOA and gas phase organic acid yields from the sequential photooxidation of seven monoterpenes, Atmos. Environ., 187, 335–345, https://doi.org/10.1016/j.atmosenv.2018.06.003, 2018.

Ghimire, R. P., Kivimäenpää, M., Blomqvist, M., Holopainen, T., Lyytikäinen-Saarenmaa, P., and Holopainen, J. K.: Effect of bark beetle (Ips typographus L.) attack on bark VOC emissions of Norway spruce (Picea abies Karst.) trees, Atmos. Environ., 126, 145–152, https://doi.org/10.1016/j.atmosenv.2015.11.049, 2016.

Gkatzelis, G. I., Coggon, M. M., McDonald, B. C., Peischl, J., Gilman, J. B., Aikin, K. C., Robinson, M. A., Canonaco, F., Prevot, A. S. H., Trainer, M., and Warneke, C.: Observations Confirm that Volatile Chemical Products Are a Major Source of Petrochemical Emissions in U.S. Cities, Environ. Sci. Technol., 55, 4332–4343, https://doi.org/10.1021/acs.est.0c05471, 2021.

Gkatzelis, G. I., Tillmann, R., Hohaus, T., Müller, M., Eichler, P., Xu, K.-M., Schlag, P., Schmitt, S. H., Wegener, R., Kaminski, M., Holzinger, R., Wisthaler, A., and Kiendler-Scharr, A.: Comparison of three aerosol chemical characterization techniques utilizing PTR-ToF-MS: a study on freshly formed and aged biogenic SOA, Atmos. Meas. Tech., 11, 1481–1500, https://doi.org/10.5194/amt-11-1481-2018, 2018.

Guenther, A. B., Jiang, X., Heald, C. L., Sakulyanontvittaya, T., Duhl, T., Emmons, L. K., and Wang, X.: The Model of Emissions of Gases and Aerosols from Nature version 2.1 (MEGAN2.1): an extended and updated framework for modeling biogenic emissions, Geosci. Model Dev., 5, 1471–1492, https://doi.org/10.5194/gmd-5-1471-2012, 2012.

Hakola, H., Hellén, H., Hemmilä, M., Rinne, J., and Kulmala, M.: In situ measurements of volatile organic compounds in a boreal forest, Atmos. Chem. Phys., 12, 11665–11678, https://doi.org/10.5194/acp-12-11665-2012, 2012.

Hakola, H., Tarvainen, V., Praplan, A. P., Jaars, K., Hemmilä, M., Kulmala, M., Bäck, J., and Hellén, H.: Terpenoid and carbonyl emissions from Norway spruce in Finland during the growing season, Atmos. Chem. Phys., 17, 3357–3370, https://doi.org/10.5194/acp-17-3357-2017, 2017.

Hallquist, M., Wenger, J. C., Baltensperger, U., Rudich, Y., Simpson, D., Claeys, M., Dommen, J., Donahue, N. M., George, C., Goldstein, A. H., Hamilton, J. F., Herrmann, H., Hoffmann, T., Iinuma, Y., Jang, M., Jenkin, M. E., Jimenez, J. L., Kiendler-Scharr, A., Maenhaut, W., McFiggans, G., Mentel, Th. F., Monod, A., Prévôt, A. S. H., Seinfeld, J. H., Surratt, J. D., Szmigielski, R., and Wildt, J.: The formation, properties and impact of secondary organic aerosol: current and emerging issues, Atmos. Chem. Phys., 9, 5155–5236, https://doi.org/10.5194/acp-9-5155-2009, 2009.

Hamilton, J. F., Webb, P. J., Lewis, A. C., and Reviejo, M. M.: Quantifying small molecules in secondary organic aerosol formed during the photo-oxidation of toluene with hydroxyl radicals, Atmos. Environ., 39, 7263–7275, https://doi.org/10.1016/j.atmosenv.2005.09.006, 2005.

Hellén, H., Praplan, A. P., Tykkä, T., Ylivinkka, I., Vakkari, V., Bäck, J., Petäjä, T., Kulmala, M., and Hakola, H.: Long-term measurements of volatile organic compounds highlight the importance of sesquiterpenes for the atmospheric chem-

istry of a boreal forest, Atmos. Chem. Phys., 18, 13839–13863, https://doi.org/10.5194/acp-18-13839-2018, 2018.

Hersbach, H., Bell, B., Berrisford, P., Hirahara, S., Horányi, A., Muñoz-Sabater, J., Nicolas, J., Peubey, C., Radu, R., Schepers, D., Simmons, A., Soci, C., Abdalla, S., Abellan, X., Balsamo, G., Bechtold, P., Biavati, G., Bidlot, J., Bonavita, M., De Chiara, G., Dahlgren, P., Dee, D., Diamantakis, M., Dragani, R., Flemming, J., Forbes, R., Fuentes, M., Geer, A., Haimberger, L., Healy, S., Hogan, R. J., Hólm, E., Janisková, M., Keeley, S., Laloyaux, P., Lopez, P., Lupu, C., Radnoti, G., de Rosnay, P., Rozum, I., Vamborg, F., Villaume, S., and Thépaut, J.-N.: The ERA5 global reanalysis, Q. J. R. Meteorol. Soc., 146, 1999–2049, https://doi.org/10.1002/qj.3803, 2020.

Huang, W., Saathoff, H., Shen, X., Ramisetty, R., Leisner, T., and Mohr, C.: Chemical Characterization of Highly Functionalized Organonitrates Contributing to Night-Time Organic Aerosol Mass Loadings and Particle Growth, Environ. Sci. Technol., 53, 1165–1174, https://doi.org/10.1021/acs.est.8b05826, 2019.

Huang, W., Li, H., Sarnela, N., Heikkinen, L., Tham, Y. J., Mikkilä, J., Thomas, S. J., Donahue, N. M., Kulmala, M., and Bianchi, F.: Measurement report: Molecular composition and volatility of gaseous organic compounds in a boreal forest – from volatile organic compounds to highly oxygenated organic molecules, Atmos. Chem. Phys., 21, 8961–8977, https://doi.org/10.5194/acp-21-8961-2021, 2021.

Isaacman-VanWertz, G., Yee, L. D., Kreisberg, N. M., Wernis, R., Moss, J. A., Hering, S. V., de Sá, S. S., Martin, S. T., Alexander, M. L., Palm, B. B., Hu, W., Campuzano-Jost, P., Day, D. A., Jimenez, J. L., Riva, M., Surratt, J. D., Viegas, J., Manzi, A., Edgerton, E., Baumann, K., Souza, R., Artaxo, P., and Goldstein, A. H.: Ambient Gas-Particle Partitioning of Tracers for Biogenic Oxidation, Environ. Sci. Technol., 50, 9952–9962, https://doi.org/10.1021/acs.est.6b01674, 2016.

Jaakkola, E., Gärtner, A., Jönsson, A. M., Ljung, K., Olsson, P.-O., and Holst, T.: Spruce bark beetles (Ips typographus) cause up to 700 times higher bark BVOC emission rates compared to healthy Norway spruce (Picea abies), Biogeosciences, 20, 803–826, https://doi.org/10.5194/bg-20-803-2023, 2023.

Jacob, D. J., Field, B. D., Jin, E. M., Bey, I., Li, Q., Logan, J. A., Yantosca, R. M., and Singh, H. B.: Atmospheric budget of acetone, J. Geophys. Res.-Atmos., 107, ACH5-1–ACH5-17, https://doi.org/10.1029/2001JD000694, 2002.

Jain, V., Tripathi, N., Tripathi, S. N., Gupta, M., Sahu, L. K., Murari, V., Gaddamidi, S., Shukla, A. K., and Prevot, A. S. H.: Real-time measurements of non-methane volatile organic compounds in the central Indo-Gangetic basin, Lucknow, India: source characterisation and their role in O3 and secondary organic aerosol formation, Atmos. Chem. Phys., 23, 3383–3408, https://doi.org/10.5194/acp-23-3383-2023, 2023.

Joó, É., Van Langenhove, H., Šimpraga, M., Steppe, K., Amelynck, C., Schoon, N., Müller, J. F., and Dewulf, J.: Variation in biogenic volatile organic compound emission pattern of Fagus sylvatica L. due to aphid infection, Atmos. Environ., 44, 227–234, https://doi.org/10.1016/j.atmosenv.2009.10.007, 2010.

Jordan, A., Haidacher, S., Hanel, G., Hartungen, E., Mark, L., Seehauser, H., Schottkowsky, R., Sulzer, P., and Mark, T. D.: A high resolution and high sensitivity proton-transfer-reaction time-of-flight mass spectrometer (PTR-TOF-MS), Int. J. Mass. Spec-

trom., 286, 122–128, https://doi.org/10.1016/j.ijms.2009.07.005, 2009.

Juráò, S., Pallozzi, E., Guidolotti, G., Fares, S., Šigut, L., Calfapietra, C., Alivernini, A., Savi, F., Veèeøová, K., Køùmal, K., Veèeøa, Z., and Urban, O.: Fluxes of biogenic volatile organic compounds above temperate Norway spruce forest of the Czech Republic, Agr. Forest Meteorol., 232, 500–513, https://doi.org/10.1016/j.agrformet.2016.10.005, 2017.

Kari, E., Miettinen, P., Yli-Pirilä, P., Virtanen, A., and Faiola, C. L.: PTR-ToF-MS product ion distributions and humidity-dependence of biogenic volatile organic compounds, Int. J. Mass. Spectrom., 430, 87–97, https://doi.org/10.1016/j.ijms.2018.05.003, 2018.

Kari, E., Faiola, C. L., Isokääntä, S., Miettinen, P., Yli-Pirilä, P., Buchholz, A., Kivimäenpää, M., Mikkonen, S., Holopainen, J. K., and Virtanen, A.: Time-resolved characterization of biotic stress emissions from Scots pines being fed upon by pine weevil by means of PTR-ToF-MS, Boreal Environ. Res., 24, 25–49, 2019.

Khare, P., Kumar, N., Kumari, K. M., and Srivastava, S. S.: Atmospheric formic and acetic acids: An overview, Rev. Geophys., 37, 227–248, https://doi.org/10.1029/1998RG900005, 1999.

Kim, S., Karl, T., Helmig, D., Daly, R., Rasmussen, R., and Guenther, A.: Measurement of atmospheric sesquiterpenes by proton transfer reaction-mass spectrometry (PTR-MS), Atmos. Meas. Tech., 2, 99–112, https://doi.org/10.5194/amt-2-99-2009, 2009.

Kleist, E., Mentel, T. F., Andres, S., Bohne, A., Folkers, A., Kiendler-Scharr, A., Rudich, Y., Springer, M., Tillmann, R., and Wildt, J.: Irreversible impacts of heat on the emissions of monoterpenes, sesquiterpenes, phenolic BVOC and green leaf volatiles from several tree species, Biogeosciences, 9, 5111–5123, https://doi.org/10.5194/bg-9-5111-2012, 2012.

Krechmer, J., Lopez-Hilfiker, F., Koss, A., Hutterli, M., Stoermer, C., Deming, B., Kimmel, J., Warneke, C., Holzinger, R., Jayne, J., Worsnop, D., Fuhrer, K., Gonin, M., and de Gouw, J.: Evaluation of a New Reagent-Ion Source and Focusing Ion–Molecule Reactor for Use in Proton-Transfer-Reaction Mass Spectrometry, Anal. Chem., 90, 12011–12018, https://doi.org/10.1021/acs.analchem.8b02641, 2018.

Lannuque, V., D'Anna, B., Kostenidou, E., Couvidat, F., Martinez-Valiente, A., Eichler, P., Wisthaler, A., Müller, M., Temime-Roussel, B., Valorso, R., and Sartelet, K.: Gas–particle partitioning of toluene oxidation products: an experimental and modeling study, Atmos. Chem. Phys., 23, 15537–15560, https://doi.org/10.5194/acp-23-15537-2023, 2023.

Lee, B. H., Lopez-Hilfiker, F. D., D'Ambro, E. L., Zhou, P., Boy, M., Petäjä, T., Hao, L., Virtanen, A., and Thornton, J. A.: Semi-volatile and highly oxygenated gaseous and particulate organic compounds observed above a boreal forest canopy, Atmos. Chem. Phys., 18, 11547–11562, https://doi.org/10.5194/acp-18-11547-2018, 2018.

Leglise, J., Müller, M., Piel, F., Otto, T., and Wisthaler, A.: Bulk Organic Aerosol Analysis by Proton-Transfer-Reaction Mass Spectrometry: An Improved Methodology for the Determination of Total Organic Mass, O:C and H:C Elemental Ratios, and the Average Molecular Formula, Anal. Chem., 91, 12619–12624, https://doi.org/10.1021/acs.analchem.9b02949, 2019.

Li, H., Riva, M., Rantala, P., Heikkinen, L., Daellenbach, K., Krechmer, J. E., Flaud, P.-M., Worsnop, D., Kulmala, M., Villenave, E.,

Perraudin, E., Ehn, M., and Bianchi, F.: Terpenes and their oxidation products in the French Landes forest: insights from Vocus PTR-TOF measurements, Atmos. Chem. Phys., 20, 1941–1959, https://doi.org/10.5194/acp-20-1941-2020, 2020.

Li, H., Canagaratna, M. R., Riva, M., Rantala, P., Zhang, Y., Thomas, S., Heikkinen, L., Flaud, P.-M., Villenave, E., Perraudin, E., Worsnop, D., Kulmala, M., Ehn, M., and Bianchi, F.: Atmospheric organic vapors in two European pine forests measured by a Vocus PTR-TOF: insights into monoterpene and sesquiterpene oxidation processes, Atmos. Chem. Phys., 21, 4123–4147, https://doi.org/10.5194/acp-21-4123-2021, 2021.

Li, X.-B., Yuan, B., Wang, S., Wang, C., Lan, J., Liu, Z., Song, Y., He, X., Huangfu, Y., Pei, C., Cheng, P., Yang, S., Qi, J., Wu, C., Huang, S., You, Y., Chang, M., Zheng, H., Yang, W., Wang, X., and Shao, M.: Variations and sources of volatile organic compounds (VOCs) in urban region: insights from measurements on a tall tower, Atmos. Chem. Phys., 22, 10567–10587, https://doi.org/10.5194/acp-22-10567-2022, 2022.

Li, Y., Zhao, J., Wang, Y., Seinfeld, J. H., and Zhang, R.: Multigeneration Production of Secondary Organic Aerosol from Toluene Photooxidation, Environ. Sci. Technol., 55, 8592–8603, https://doi.org/10.1021/acs.est.1c02026, 2021.

Luo, H., Guo, Y., Shen, H., Huang, D. D., Zhang, Y., and Zhao, D.: Effect of relative humidity on the molecular composition of secondary organic aerosols from α-pinene ozonolysis, Environ. Sci.-Atmos., 4, 519–530, https://doi.org/10.1039/D3EA00149K, 2024.

Mermet, K., Perraudin, E., Dusanter, S., Sauvage, S., Léonardis, T., Flaud, P.-M., Bsaibes, S., Kammer, J., Michoud, V., Gratien, A., Cirtog, M., Al Ajami, M., Truong, F., Batut, S., Hecquet, C., Doussin, J.-F., Schoemaecker, C., Gros, V., Locoge, N., and Villenave, E.: Atmospheric reactivity of biogenic volatile organic compounds in a maritime pine forest during the LANDEX episode 1 field campaign, Sci. Total Environ., 756, 144129, https://doi.org/10.1016/j.scitotenv.2020.144129, 2021.

Mohr, C., Lopez-Hilfiker, F. D., Yli-Juuti, T., Heitto, A., Lutz, A., Hallquist, M., D'Ambro, E. L., Rissanen, M. P., Hao, L., Schobesberger, S., Kulmala, M., Mauldin III, R. L., Makkonen, U., Sipilä, M., Petäjä, T., and Thornton, J. A.: Ambient observations of dimers from terpene oxidation in the gas phase: Implications for new particle formation and growth, Geophys. Res. Lett., 44, 2958–2966, https://doi.org/10.1002/2017GL072718, 2017.

Montzka, C., Bayat, B., Tewes, A., Mengen, D., and Vereecken, H.: Sentinel-2 Analysis of Spruce Crown Transparency Levels and Their Environmental Drivers After Summer Drought in the Northern Eifel (Germany), Front. For. Glob. Chang., 4, 667151, https://doi.org/10.3389/ffgc.2021.667151, 2021.

Müller, M., Eicher, P., D'Anna, B., Tan, W., and Wisthaler, A.: Direct Sampling and Analysis of Atmospheric Particulate Organic Matter by Proton-Transfer-Reaction Mass Spectrometry, Anal. Chem., 89, 10889–10897, https://doi.org/10.1021/acs.analchem.7b02582, 2017.

Ng, N. L., Canagaratna, M. R., Zhang, Q., Jimenez, J. L., Tian, J., Ulbrich, I. M., Kroll, J. H., Docherty, K. S., Chhabra, P. S., Bahreini, R., Murphy, S. M., Seinfeld, J. H., Hildebrandt, L., Donahue, N. M., DeCarlo, P. F., Lanz, V. A., Prévôt, A. S. H., Dinar, E., Rudich, Y., and Worsnop, D. R.: Organic aerosol components observed in Northern Hemispheric datasets from Aerosol Mass Spectrometry, Atmos. Chem. Phys., 10, 4625–4641, https://doi.org/10.5194/acp-10-4625-2010, 2010.

Ng, N. L., Canagaratna, M. R., Jimenez, J. L., Chhabra, P. S., Seinfeld, J. H., and Worsnop, D. R.: Changes in organic aerosol composition with aging inferred from aerosol mass spectra, Atmos. Chem. Phys., 11, 6465–6474, https://doi.org/10.5194/acp-11-6465-2011, 2011.

Paatero, P. and Tapper, U.: Positive matrix factorization: A non-negative factor model with optimal utilization of error estimates of data values, Environmetrics, 5, 111–126, https://doi.org/10.1002/env.3170050203, 1994.

Pagonis, D., Sekimoto, K., and de Gouw, J.: A Library of Proton-Transfer Reactions of H3O+ Ions Used for Trace Gas Detection, J. Am. Soc. Mass Spectrom., 30, 1330–1335, https://doi.org/10.1007/s13361-019-02209-3, 2019.

Papurello, D., Soukoulis, C., Schuhfried, E., Cappellin, L., Gasperi, F., Silvestri, S., Santarelli, M., and Biasioli, F.: Monitoring of volatile compound emissions during dry anaerobic digestion of the Organic Fraction of Municipal Solid Waste by Proton Transfer Reaction Time-of-Flight Mass Spectrometry, Bioresour. Technol., 126, 254–265, https://doi.org/10.1016/j.biortech.2012.09.033, 2012.

Peng, Y., Wang, H., Gao, Y., Jing, S., Zhu, S., Huang, D., Hao, P., Lou, S., Cheng, T., Huang, C., and Zhang, X.: Real-time measurement of phase partitioning of organic compounds using a proton-transfer-reaction time-of-flight mass spectrometer coupled to a CHARON inlet, Atmos. Meas. Tech., 16, 15–28, https://doi.org/10.5194/amt-16-15-2023, 2023.

Peñuelas, J. and Staudt, M.: BVOCs and global change, Trends Plant Sci., 15, 133–144, 2010.

Pernov, J. B., Bossi, R., Lebourgeois, T., Nøjgaard, J. K., Holzinger, R., Hjorth, J. L., and Skov, H.: Atmospheric VOC measurements at a High Arctic site: characteristics and source apportionment, Atmos. Chem. Phys., 21, 2895–2916, https://doi.org/10.5194/acp-21-2895-2021, 2021.

Peron, A., Kaser, L., Fitzky, A. C., Graus, M., Halbwirth, H., Greiner, J., Wohlfahrt, G., Rewald, B., Sandén, H., and Karl, T.: Combined effects of ozone and drought stress on the emission of biogenic volatile organic compounds from Quercus robur L., Biogeosciences, 18, 535–556, https://doi.org/10.5194/bg-18-535-2021, 2021.

Petersen, R., Holst, T., Mölder, M., Kljun, N., and Rinne, J.: Vertical distribution of sources and sinks of volatile organic compounds within a boreal forest canopy, Atmos. Chem. Phys., 23, 7839–7858, https://doi.org/10.5194/acp-23-7839-2023, 2023.

Piel, F., Müller, M., Winkler, K., Skytte af Sätra, J., and Wisthaler, A.: Introducing the extended volatility range proton-transfer-reaction mass spectrometer (EVR PTR-MS), Atmos. Meas. Tech., 14, 1355–1363, https://doi.org/10.5194/amt-14-1355-2021, 2021.

Rasmussen, R. A. and Went, F.: Volatile organic material of plant origin in the atmosphere, P. Natl. Acad. Sci. USA, 53, 215–220, 1965.

Salazar Gómez, J. I., Lohmann, H., and Krassowski, J.: Determination of volatile organic compounds from biowaste and co-fermentation biogas plants by single-sorbent adsorption, Chemosphere, 153, 48–57, https://doi.org/10.1016/j.chemosphere.2016.02.128, 2016.

Scheftelowitz, M., Becker, R., and Thrän, D.: Improved power provision from biomass: A retrospective on the impacts of German energy policy, Biomass Bioenerg., 111, 1–12, https://doi.org/10.1016/j.biombioe.2018.01.010, 2018.

Shrivastava, M., Cappa, C. D., Fan, J., Goldstein, A. H., Guenther, A. B., Jimenez, J. L., Kuang, C., Laskin, A., Martin, S. T., Ng, N. L., Petaja, T., Pierce, J. R., Rasch, P. J., Roldin, P., Seinfeld, J. H., Shilling, J., Smith, J. N., Thornton, J. A., Volkamer, R., Wang, J., Worsnop, D. R., Zaveri, R. A., Zelenyuk, A., and Zhang, Q.: Recent advances in understanding secondary organic aerosol: Implications for global climate forcing, Rev. Geophys., 55, 509–559, https://doi.org/10.1002/2016RG000540, 2017.

Sindelarova, K., Granier, C., Bouarar, I., Guenther, A., Tilmes, S., Stavrakou, T., Müller, J.-F., Kuhn, U., Stefani, P., and Knorr, W.: Global data set of biogenic VOC emissions calculated by the MEGAN model over the last 30 years, Atmos. Chem. Phys., 14, 9317–9341, https://doi.org/10.5194/acp-14-9317-2014, 2014.

Smiatek, G. and Steinbrecher, R.: Temporal and spatial variation of forest VOC emissions in Germany in the decade 1994–2003, Atmos. Environ., 40, 166–177, https://doi.org/10.1016/j.atmosenv.2005.11.071, 2006.

Song, J., Saathoff, H., Gao, L., Gebhardt, R., Jiang, F., Vallon, M., Bauer, J., Norra, S., and Leisner, T.: Variations of $PM_{2.5}$ sources in the context of meteorology and seasonality at an urban street canyon in Southwest Germany, Atmos. Environ., 119147, https://doi.org/10.1016/j.atmosenv.2022.119147, 2022.

Song, J., Saathoff, H., Jiang, F., Gao, L., Zhang, H., and Leisner, T.: Sources of organic gases and aerosol particles and their roles in nighttime particle growth at a rural forested site in southwest Germany, Atmos. Chem. Phys., 24, 6699–6717, https://doi.org/10.5194/acp-24-6699-2024, 2024a.

Song, J., Gkatzelis, G., Tillmann, R., Brüggemann, N., Leisner, T., and Saathoff, H.: Data of Characterization of biogenic volatile organic compounds and their oxidation products at a stressed pine forest close to a biogas power plant, Karlsruhe Institute of Technology [data set], https://doi.org/10.35097/qbwwf0p62zksrkwj, 2024b.

Surdu, M., Lamkaddam, H., Wang, D. S., Bell, D. M., Xiao, M., Lee, C. P., Li, D., Caudillo, L., Marie, G., Scholz, W., Wang, M., Lopez, B., Piedehierro, A. A., Ataei, F., Baalbaki, R., Bertozzi, B., Bogert, P., Brasseur, Z., Dada, L., Duplissy, J., Finkenzeller, H., He, X.-C., Höhler, K., Korhonen, K., Krechmer, J. E., Lehtipalo, K., Mahfouz, N. G. A., Manninen, H. E., Marten, R., Massabò, D., Mauldin, R., Petäjä, T., Pfeifer, J., Philippov, M., Rörup, B., Simon, M., Shen, J., Umo, N. S., Vogel, F., Weber, S. K., Zauner-Wieczorek, M., Volkamer, R., Saathoff, H., Möhler, O., Kirkby, J., Worsnop, D. R., Kulmala, M., Stratmann, F., Hansel, A., Curtius, J., Welti, A., Riva, M., Donahue, N. M., Baltensperger, U., and El Haddad, I.: Molecular Understanding of the Enhancement in Organic Aerosol Mass at High Relative Humidity, Environ. Sci. Technol., 57, 2297–2309, https://doi.org/10.1021/acs.est.2c04587, 2023.

Tani, A., Hayward, S., and Hewitt, C. N.: Measurement of monoterpenes and related compounds by proton transfer reaction-mass spectrometry (PTR-MS), Int. J. Mass. Spectrom., 223–224, 561–578, https://doi.org/10.1016/S1387-3806(02)00880-1, 2003.

Teskey, R., Wertin, T., Bauweraerts, I., Ameye, M., McGuire, M. A., and Steppe, K.: Responses of tree species to heat waves and extreme heat events, Plant Cell Environ., 38, 1699–1712, https://doi.org/10.1111/pce.12417, 2015.

Tillmann, R., Hallquist, M., Jonsson, Å. M., Kiendler-Scharr, A., Saathoff, H., Iinuma, Y., and Mentel, Th. F.: Influence of relative humidity and temperature on the production of pinonaldehyde and OH radicals from the ozonolysis of α-pinene, Atmos. Chem. Phys., 10, 7057–7072, https://doi.org/10.5194/acp-10-7057-2010, 2010.

Trainer, M., Williams, E. J., Parrish, D. D., Buhr, M. P., Allwine, E. J., Westberg, H. H., Fehsenfeld, F. C., and Liu, S. C.: Models and observations of the impact of natural hydrocarbons on rural ozone, Nature, 329, 705–707, https://doi.org/10.1038/329705a0, 1987.

van Meeningen, Y., Schurgers, G., Rinnan, R., and Holst, T.: Isoprenoid emission response to changing light conditions of English oak, European beech and Norway spruce, Biogeosciences, 14, 4045–4060, https://doi.org/10.5194/bg-14-4045-2017, 2017.

Vermeuel, M. P., Novak, G. A., Kilgour, D. B., Claflin, M. S., Lerner, B. M., Trowbridge, A. M., Thom, J., Cleary, P. A., Desai, A. R., and Bertram, T. H.: Observations of biogenic volatile organic compounds over a mixed temperate forest during the summer to autumn transition, Atmos. Chem. Phys., 23, 4123–4148, https://doi.org/10.5194/acp-23-4123-2023, 2023.

Vestenius, M., Hopke, P. K., Lehtipalo, K., Petäjä, T., Hakola, H., and Hellén, H.: Assessing volatile organic compound sources in a boreal forest using positive matrix factorization (PMF), Atmos. Environ., 259, 118503, https://doi.org/10.1016/j.atmosenv.2021.118503, 2021.

von Hessberg, C., von Hessberg, P., Pöschl, U., Bilde, M., Nielsen, O. J., and Moortgat, G. K.: Temperature and humidity dependence of secondary organic aerosol yield from the ozonolysis of β-pinene, Atmos. Chem. Phys., 9, 3583–3599, https://doi.org/10.5194/acp-9-3583-2009, 2009.

Wang, L., Slowik, J. G., Tripathi, N., Bhattu, D., Rai, P., Kumar, V., Vats, P., Satish, R., Baltensperger, U., Ganguly, D., Rastogi, N., Sahu, L. K., Tripathi, S. N., and Prévôt, A. S. H.: Source characterization of volatile organic compounds measured by proton-transfer-reaction time-of-flight mass spectrometers in Delhi, India, Atmos. Chem. Phys., 20, 9753–9770, https://doi.org/10.5194/acp-20-9753-2020, 2020.

Weber, J., Archer-Nicholls, S., Abraham, N. L., Shin, Y. M., Griffiths, P., Grosvenor, D. P., Scott, C. E., and Archibald, A. T.: Chemistry-driven changes strongly influence climate forcing from vegetation emissions, Nat. Commun., 13, 7202, https://doi.org/10.1038/s41467-022-34944-9, 2022.

Wennberg, P. O., Bates, K. H., Crounse, J. D., Dodson, L. G., McVay, R. C., Mertens, L. A., Nguyen, T. B., Praske, E., Schwantes, R. H., Smarte, M. D., St Clair, J. M., Teng, A. P., Zhang, X., and Seinfeld, J. H.: Gas-Phase Reactions of Isoprene and Its Major Oxidation Products, Chem. Rev., 118, 3337–3390, https://doi.org/10.1021/acs.chemrev.7b00439, 2018.

Wu, R., Pan, S., Li, Y., and Wang, L.: Atmospheric Oxidation Mechanism of Toluene, J. Phys. Chem. A, 118, 4533–4547, https://doi.org/10.1021/jp500077f, 2014.

Yáñez-Serrano, A. M., Bourtsoukidis, E., Alves, E. G., Bauwens, M., Stavrakou, T., Llusià, J., Filella, I., Guenther, A., Williams, J., Artaxo, P., Sindelarova, K., Doubalova, J., Kesselmeier, J., and Peñuelas, J.: Amazonian biogenic volatile organic com-

pounds under global change, Glob. Change Biol., 26, 4722–4751, https://doi.org/10.1111/gcb.15185, 2020.

Yáñez-Serrano, A. M., Bach, A., Bartolomé-Català, D., Matthaios, V., Seco, R., Llusià, J., Filella, I., and Peñuelas, J.: Dynamics of volatile organic compounds in a western Mediterranean oak forest, Atmos. Environ., 257, 118447, https://doi.org/10.1016/j.atmosenv.2021.118447, 2021.

Yatavelli, R. L. N., Stark, H., Thompson, S. L., Kimmel, J. R., Cubison, M. J., Day, D. A., Campuzano-Jost, P., Palm, B. B., Hodzic, A., Thornton, J. A., Jayne, J. T., Worsnop, D. R., and Jimenez, J. L.: Semicontinuous measurements of gas–particle partitioning of organic acids in a ponderosa pine forest using a MOVI-HRToF-CIMS, Atmos. Chem. Phys., 14, 1527–1546, https://doi.org/10.5194/acp-14-1527-2014, 2014.

Zaytsev, A., Koss, A. R., Breitenlechner, M., Krechmer, J. E., Nihill, K. J., Lim, C. Y., Rowe, J. C., Cox, J. L., Moss, J., Roscioli, J. R., Canagaratna, M. R., Worsnop, D. R., Kroll, J. H., and Keutsch, F. N.: Mechanistic study of the formation of ring-retaining and ring-opening products from the oxidation of aromatic compounds under urban atmospheric conditions, Atmos. Chem. Phys., 19, 15117–15129, https://doi.org/10.5194/acp-19-15117-2019, 2019.

Zhang, X., McVay, R. C., Huang, D. D., Dalleska, N. F., Aumont, B., Flagan, R. C., and Seinfeld, J. H.: Formation and evolution of molecular products in α-pinene secondary organic aerosol, P. Natl. Acad. Sci. USA, 112, 14168–14173, https://doi.org/10.1073/pnas.1517742112, 2015